Seasonal impact of biogenic very short-lived bromine on lowermost stratospheric ozone between 60º N and 60º S during the 21st century

Javier Alejandro Barrera[1], Rafael Pedro Fernandez[1,2,3], Fernando Iglesias-Suarez[2], Carlos Alberto Cuevas[2], Jean-Francois Lamarque[4] and Alfonso Saiz-Lopez[2]

[1] Institute for Interdisciplinary Science, National Research Council (ICB-CONICET), FCEN-UNCuyo, Mendoza, 5500, Argentina
[2] Department of Atmospheric Chemistry and Climate, Institute of Physical Chemistry Rocasolano, CSIC, Madrid, 28006, Spain
[3] Atmospheric and Environmental Studies Group (GEAA), UTN-FRM, Mendoza, 5500, Argentina
[4] Atmospheric Chemistry, Observations & Modelling Laboratory, National Center for Atmospheric Research, Boulder, CO 80301, USA

Correspondence to: Alfonso Saiz-Lopez & Rafael P. Fernandez (a.saiz@csic.es; rpfernandez@conicet.gov.ar)

Abstract. Biogenic very short-lived bromine (VSL^{Br}) represents, nowadays, ~25% of the total stratospheric bromine loading. Owing to their much shorter lifetime compared to anthropogenic long-lived bromine (e.g., halons) and chlorine (e.g., chlorofluorocarbons), the impact of VSL^{Br} on ozone peaks in the lowermost stratosphere, which is a key climatic and radiative atmospheric region. Here we present a modelling study of the evolution of stratospheric ozone and its chemical losses within the tropics and mid-latitudes during the 21st century. Two different experiments are explored: considering and neglecting the additional stratospheric injection of 5 ppt biogenic VSL^{Br} naturally released from the ocean. Our analysis shows that the inclusion of VSL^{Br} results in a realistic stratospheric bromine loading and improves the agreement between the model and satellite observations of total ozone column (TOC) for the 1980-2015 period at the mid-latitudes. We show that the overall ozone response to VSL^{Br} within the mid-latitudes follows the stratospheric evolution of long-lived inorganic chlorine and bromine throughout the 21st century. Additional ozone losses due to VSL^{Br} are maximised during the present-day period (1990-2010), with TOC differences of −8 DU (−3 %) and −5.5 DU (−2 %) for the southern (SH-ML) and northern (NH-ML) mid-latitudes, respectively. Moreover, the projected TOC differences at the end of the 21st century are ~50 % lower than the values found for the present-day period.

We find that the seasonal VSL^{Br} impacts on mid-latitude lowermost stratospheric ozone are influenced by the seasonality of the inorganic chlorine heterogeneous reactivation processes on ice-crystals. Indeed, due to the more efficient reactivation of chlorine reservoirs (mainly $ClONO_2$ and HCl) within the colder SH-ML lowermost stratosphere, the seasonal VSL^{Br} impact shows a small but persistent hemispheric asymmetry through the whole modelled period. Our results indicate that, although the overall VSL^{Br}-driven ozone destruction is largest during spring, the halogen-mediated ($Halog_{x-Loss}$) ozone loss cycle in the mid-latitude lowermost stratosphere during winter is comparatively more efficient than the HO_x cycle with respect to other seasons. Indeed, when VSL^{Br} are considered, $Halog_{x-Loss}$ dominates wintertime lowermost stratospheric ozone loss at the SH-ML between 1985 and 2020, with a contribution of inter-halogen ClO_x–BrO_x cycles to $Halog_{x-Loss}$ of ~50 %.

Within the tropics, a small (< –2.5 DU) and relatively constant (~ –1 %) ozone depletion mediated by VSL-bromine is closely related to its fixed emissions throughout the modelled period. By including the VSL^{Br} sources, the seasonal $Halog_{x-Loss}$ contribution to lowermost stratospheric ozone loss is practically dominated by the BrO_x cycle, reflecting the low sensitivity of VSL-bromine to background halogen abundances to drive the tropical stratospheric

ozone depletion. We conclude that considering the coupling between biogenic bromine sources and seasonal changes of the chlorine heterogeneous reactivation is a key feature for future projections of mid-latitude lowermost stratospheric ozone during the 21st century.

1 Introduction

The role of bromine in stratospheric ozone depletion has been discussed in several studies (Wofsy et al., 1975; Prather and Watson, 1990; Daniel et al., 1999; Dvortsov et al., 1999; Solomon et al., 1999). Although bromine is much less abundant than chlorine in the atmosphere, it is known to deplete stratospheric ozone 45 to 69 times more efficiently on a per atom basis (Daniel et al., 1999; Sinnhuber et al., 2009). Moreover, the ozone depletion efficiency of active bromine (Br and BrO) is strongly related to the available amount of activated chlorine (manly Cl and ClO radicals) in the atmosphere (McElroy et al., 1986; Solomon et al., 1999, and references therein) as well as with enhanced sulphate aerosol loading, via heterogeneous reactions (Salawitch et al., 2005). Consequently, even low concentrations of bromine have a relatively large impact on stratospheric ozone. In addition to anthropogenic long-lived chlorine (LL^{Cl}) and bromine (LL^{Br}) substances, such as chlorofluorocarbons (CFCs), chlorocarbons, methyl bromide and bromofluorocarbons (halon fire suppressants), other substances with photochemical lifetimes shorter than 6 months, often referred to as very short-lived substances (VSL), have the potential to transport a significant amount of reactive halogens into the stratosphere. Owing to their short lifetimes, the impact of VSL on stratospheric ozone peaks at the lowermost stratosphere (Salawitch et al., 2005; Feng et al., 2007; Sinnhuber et al., 2009, 2015; Yang et al., 2014; Hossaini et al., 2015a; Falk et al., 2017), which is an important atmospheric region because surface temperature and climate are most sensitive to ozone perturbations (Riese et al., 2012; Hossaini et al., 2015b, Iglesias-Suarez et al., 2018). In fact, Hossaini et al. (2015b) found that very short-lived bromine (VSL^{Br}) exert a 3.6 times larger ozone radiative effect (normalized by halogen content) than that arising from long-lived substances.

VSL^{Br} are produced in the ocean, via the metabolism of marine organisms such as phytoplankton and macroalgae (e.g. Carpenter et al., 2007; Quack et al., 2007; Leedham Elvidge et al., 2015), even in sea-ice (e.g. Abrahamsson et al., 2018). Due to their high volatility, they are transferred into the marine boundary layer through air-sea exchange (Carpenter and Liss, 2000; Quack and Wallace, 2003). The most abundant VSL^{Br} compounds released to the atmosphere are bromoform ($CHBr_3$) and dibromomethane (methylene dibromide, CH_2Br_2), followed by minor (but not-negligible) contribution of inter-halogen species (bromochloromethane, CH_2BrCl; dibromochloromethane, $CHBr_2Cl$ and bromodichloromethane, $CHBrCl_2$). Altogether, VSL^{Br} contribute with ~ 5 (3–7) ppt to stratospheric bromine, which accounts for about 25% of total stratospheric bromine in 2016 (World Meteorological Organization (WMO), 2018). Moreover, this additional input of bromine is required to reconcile current stratospheric bromine trends (Salawitch et al., 2010; WMO, 2018).

Production of anthropogenic LL^{Cl} and LL^{Br} substances has been restricted by the Montreal Protocol and its subsequent amendments and adjustments (Solomon et al., 1999; WMO, 2018). After application, the stratospheric LL^{Cl} and LL^{Br} load has peaked at the end of the 20th century and is decreasing at a rate that depends on their respective atmospheric lifetimes. This imply, for example, that hydrogen chloride (HCl) shows a long-term decrease at a rate of about 0.5 % yr^{-1} in the middle stratosphere between 60ºN and 60ºS, while total stratospheric bromine decreases at a rate of about 0.75% yr^{-1} from 2004 to 2014 (WMO 2018). Accordingly, stratospheric ozone

is expected to recover from the effects of anthropogenic halogen-induced loss on a similar timescale, which is already detectable in the Antarctic and upper stratosphere (e.g. Solomon et al., 2016a; Chipperfield et al., 2017; Dhomse et al. 2018; Strahan and Douglass, 2008, and references therein). Hossaini et al. (2015a), quantified the stratospheric injection of organic and inorganic chlorine from anthropogenic VSL^{Cl} sources such as chloroform ($CHCl_3$), dichloromethane (CH_2Cl_2), tetrachloroethene (C_2Cl_4), trichloroethene (C_2HCl_3), and 1,2-dichloroethane (CH_2ClCH_2Cl), which are not controlled by the Montreal Protocol. From their results, the total stratospheric chlorine load from VSL^{Cl} inferred for 2013 is 123 ppt, with a stratospheric injection dominated by source gases (~ 83%). Moreover, the stratospheric VSL-chlorine (organic and inorganic) injection increased by ~ 52% between 2005 and 2013, mainly due to a recent and ongoing growth in anthropogenic CH_2Cl_2 emissions. In fact, Hossaini et al. (2017), showed that the impact of CH_2Cl_2 on stratospheric ozone has increased markedly in recent years and if these increases continue into the future, the recovery of Earth's ozone layer could be delayed even further, offsetting some of the gains achieved by the Montreal Protocol.

The total stratospheric chlorine and bromine budget derived for 2016 were 3.29 ppb Cl and 19.60 ppt Br, respectively (WMO, 2018), and are expected to return to their 1980 values, an arbitrary reference date before the discovery of the Antarctic ozone hole, around the middle of this century (Dhomse et al. 2018). Although we still lack a scientific consensus with respect to the future evolution of VSL^{Br} oceanic source strength and stratospheric injection (WMO, 2014; Lennartz et al., 2015; Ziska et al., 2017), the continuous decrease of LL^{Br} leads to an increase in the relative VSL^{Br} contribution to total stratospheric bromine into the future. Thus, understanding the role of natural VSL^{Br} sources is a key issue for chemistry-climate projections.

The impact of additional bromine is closely related to the heterogeneous chemistry of chlorine (Solomon et al., 1999; Salawitch et al., 2005; Müller, 2012). The influence of temperature and water vapour in the heterogeneous conversion processes of inorganic chlorine reservoirs (mostly HCl and $ClONO_2$) into active radicals on sulphate aerosols, has been reviewed elsewhere (e.g. Anderson et al., 2012, 2017; Drdla and Müller, 2012; Anderson and Clapp, 2018). In particular, Drdla and Müller (2012) highlighted that an increase in water vapour above background values would allow chlorine activation at higher temperatures than those observed in polar regions, which led to the hypothesis that chlorine reactivation and subsequent ozone loss could occur in the lower stratosphere at mid-latitudes during summer (Robertrech et al., 2019). Indeed, the spatial and seasonal distributions of chlorine monoxide and chlorine nitrate in the monsoon regions provide indicators of heterogeneous chlorine processing in the tropical and subtropical lowermost stratosphere of the northern hemisphere (Solomon et al., 2016b). Moreover, heterogeneous chorine reactivation has also been observed on ice-particles in cirrus clouds located near the tropopause (Borrman et al., 1996, 1997; Solomon et al., 1997; Bregman et al, 2002; Thornton et al., 2003). The occurrence of cirrus clouds was reported in the lowermost stratosphere of northern high-mid latitudes (40–75º N) (Spang et al., 2015), with summertime clouds located up to ~3 km (or 40–50 K of potential temperature) above the tropopause (Dressler, 2009). Also, von Hobe et al. (2011) suggested that cirrus ice particles at low temperatures may promote a significant activation of heterogeneous chlorine in the tropical upper troposphere lower stratosphere. Finally, satellite observations indicate that chlorine activation also occurs in the Antarctic and Arctic subvortex regions, where processed air dispersing from the decaying vortex in spring induces rapid changes in extravortex trace gas abundances (Santee et al., 2011).

Previous chemistry-climate modelling studies considering VSL^{Br} chemistry mainly focused on improving the model vs. observed mid-latitude ozone trends at the end of the 20th century (Feng et al., 2007; Sinnhuber et al., 2009). More recently, Sinnhuber and Meul (2015) have shown a much larger ozone depletion in the lowermost stratosphere during the 1979–1995 period and a greater ozone increase during 1996–2005 period, in better agreement with observations, due to inclusion of VSL^{Br} sources. Moreover, Falk et al. (2017) have reported that the projected additional VSL^{Br} impact on ozone at the end of the 21st century is reduced compared to present day. This result are in agreement with that of Yang et al. (2014), who performed time-slice simulations to address the sensitivity of stratospheric ozone to a speculative doubling of VSL^{Br} sources under different LL^{Cl} scenarios. However, neither of the previous studies had distinguished the ozone depleting contribution – including its seasonal variability– that arises from VSL^{Br} respect to LL^{Cl} and LL^{Br} throughout the 21st century.

In this work, using the CAM-Chem model, we present a coupled chemistry-climate modelling study from 1960 to 2100 with and without the contribution from VSL^{Br} sources. We focus on natural VSL^{Br}-driven impacts on the temporal evolution of stratospheric ozone and total ozone column (TOC) in the tropics and mid-latitudes, distinguishing both the long-term seasonal change and the resulting hemispheric asymmetries. Additionally, we present a timeline assessment of the individual contribution from anthropogenic (LL^{Cl} and LL^{Br}) and biogenic (VSL^{Br}) sources to stratospheric halogen loading throughout the 21st century, recognizing also the VSL^{Br} contribution to the overall halogen-catalysed ozone losses in the lowermost stratosphere. The layout of the paper is as follows: Section 2 describes the main characteristics and configuration of the CAM-Chem model, as well as the observation data sets that are used for the evaluation of the CAM-Chem performance. Section 3 presents a quantitative comparison between the model and observations of stratospheric chlorine and bromine loading (3.1) and TOC (3.2), as well as discusses long-term seasonal impacts mediated by VSL^{Br} on TOC (3.2) and lowermost stratospheric ozone budget (3.3). Changes in the seasonal evolution of halogen-driven ozone loss rates due to VSL^{Br} are shown in section 3.4. The final concluding remarks are summarized in Section 4.

2 Methods: model description

The Community Earth System Model (CESM1) with the Community Atmospheric Model including interactive chemistry (CAM4-Chem version; Lamarque et al., 2012; Tilmes et al., 2016) has been used to explore VSL^{Br}-driven stratospheric ozone loss on three latitude bands: southern hemisphere mid-latitudes (SH-ML; 60–35º S), tropics (tropics; 25º N–25º S) and northern hemisphere mid-latitudes (NH-ML; 35–60º N). The model setup follows the Chemistry-Climate Model Initiative (CCMI) REFC2 configuration described in detail by Tilmes et al. (2016), with the exception that in this work we consider a full halogen chemistry mechanism and oceanic emission –seasonal-dependent and geographically distributed– of six bromocarbons (VSL^{Br}= $CHBr_3$, CH_2Br_2, CH_2BrCl, $CHBrCl_2$, $CHBr_2Cl$ and CH_2IBr) from Ordóñez et al., (2012) emission inventory. This emission inventory is based on a monthly-varying satellite chl-a climatology, which allows to introduce a complete seasonal cycle to the emission strength and spatial distribution of oceanic bromocarbons. A full description of the VSL^{Br} mechanism implemented in CAM-Chem, including both biogenic and anthropogenic sources, heterogeneous recycling reactions, dry and wet deposition, convective uplift and large-scale transport has been given elsewhere (Ordóñez et al., 2012; Fernandez et al., 2014). Monthly and seasonally varying lower boundary conditions were considered for long-lived chlorine (LL^{Cl} = CH_3Cl, CH_3CCl_3, CCl_4, CFC–11, CFC–12, CFC–113, HCFC–22, CFC–114,

CFC–115, HCFC–141b, HCFC–142b) and long–lived bromine (LL^{Br} = CH_3Br, H–1301, H–1211, H–1202, and H–2402), following the A1 halogenated ozone–depleting substances emissions scenario from WMO Ozone Assessment Report (2011). The surface concentrations of CO_2, CH_4, H_2 and N_2O were specified following the moderate Representation Concentration Pathway 6.0 (RCP6.0) scenario (Meinshausen et al., 2011; Eyring et al., 2013).

The CAM-Chem configuration used in this work extends from the surface to approximately 40 km (3.5 hPa in the upper stratosphere) with 26 vertical levels and includes a horizontal resolution of 1.9º latitude by 2.5º longitude. The number of stratospheric levels changes depending on the latitudinal region: within the tropics, there are eight levels above the tropopause (~100 hPa), with a mean thickness of 1.25 km (15.5 hPa) for the lower stratospheric levels and 5.2 km (3.8 hPa) between the two highest levels; while for the mid-latitudes, the tropopause is located approximately at ~200 hPa, and the stratosphere contains up to 12 levels. To ensure a consistent dynamical description of the stratosphere within the relatively low model top of CAM-Chem (i.e., gravity-wave dragging and the Brewer-Dobson circulation), the integrated momentum that would have been deposited above the model top is specified by an upper boundary condition (Lamarque et al., 2008). A similar procedure is applied to the altitude-dependent photolysis rate computations, which include an upper boundary condition that considers the ozone column fraction prevailing above the model top. The CAM4-Chem version used in this work includes a non-orographic gravity wave scheme based on the inertia-gravity wave parameterization and an observational-based implementation of stratospheric aerosol and surface area density. The quasi-biennial oscillation is imposed in the model by relaxing equatorial zonal winds between 90 to 3 hPa to the observed interannual variability (see Tilmes et al., 2016 for more details).

Equivalent CAM-Chem configurations, as the one implemented in this work, have been used for the CCMVal-2 (Chemistry-Climate Model Validation 2) and CMIP5 (Coupled Model Intercomparison Project, Phase 5) activities, in order to represent trends in the ozone evolution and to estimate the return dates, which lie in the middle of the multi-model range (Eyring et al., 2010; 2013). Moreover, our model configuration uses a fully coupled Earth System Model approach, i.e. the ocean and sea ice are explicitly computed (Neale et al.,2013). This implies that instead of isolating the chemical impact mediated by VSL^{Br} sources on the climatological ozone budget (as would be the case using a specified dynamic approach), the chemical interaction between VSL-bromine and ozone in the lowermost stratosphere is affected by dynamic feedbacks (i.e. temperature, radiation, etc.).

Even though the interactive ocean coupling would have allowed us to compute the evolution of VSL^{Br} ocean source emissions throughout the modelled period, we still lack a considerable understanding of the seasonal processes that dominate VSL^{Br} ocean emissions in both present and future time, which is combined with a limited observation data set on VSL bromocarbons (WMO, 2014; WMO, 2018). Therefore, in this work, we forced the model with annually-cycled VSL^{Br} fluxes, replicating the Ordoñez et al. emissions inventory for all years between 1950 and 2100. This procedure aims to reduce the uncertainties associated with the unknown evolution of both biogeochemical production and oceanic emissions of VSL^{Br} into the future (Lennartz et al.; 2015; Ziska et al., 2017).

Two ensembles of independent modelled experiments were performed, each with three individual simulations from 1960 to 2100, considering approximately 10-year of spin-up to allow stabilization of the stratospheric circulation. The individual simulations 001,002 and 003 started in 1950, 1951 and 1952, respectively, with initial conditions

taken from the equivalent years of the CESM1-WACCM (Whole Atmosphere Community Climate Model) 20th century ensemble for CMIP5 (Marsh et al., 2013). The baseline simulations set-up of first experiment considered only the halogen LL^{Cl} and LL^{Br} contribution from anthropogenic chlorofluorocarbons, hydrochlorofluorocarbons, halons, methyl chloride and methyl bromide; while the simulations set-up of second experiment included, in addition to the above anthropogenic sources, the background biogenic contribution from VSL^{Br} oceanic sources. The mean ensemble of each experiment (i.e. with and without the VSL^{Br} sources) was calculated as the average of the three individual simulations. Differences between these two mean ensembles allow quantification of the overall impact of VSL^{Br} sources on stratospheric ozone, as well as to determine their relative contributions to the halogen mediated catalytic ozone depleting families. In addition, from this analysis it is also possible to distinguish the contributions of both LL^{Br} and VSL^{Br} to the inorganic fraction of stratospheric bromine ($Br_y^{LL+VSL} = Br_y^{LL} + Br_y^{VSL}$ = Br + BrO + HBr + $BrONO_2$ + BrCl + HOBr + $2Br_2$ + $BrNO_2$), whereas the inorganic fraction of chlorine (Cl_y^{LL} = ClO + Cl + HOCl + $2Cl_2O_2$ + $2Cl_2$ + OClO + HCl + $ClONO_2$ + BrCl + $ClONO_2$) arises only from the degradation of LL^{Cl} which is identical for both experiments.

For the case of vertical distributions and latitudinal variations, the zonal mean of each mean ensemble was computed from the monthly output before processing the data, while a Lowess filter with a 0.2 fraction was applied to all long-term time series to smooth the data. Most of the figures and values within the Results section include geographically averaged quantities for present-day (defined here as the 1990–2010 mean, nominally year 2000) and the end of the 21st century (defined here as the 2080–2100 mean, nominally year 2100) periods over the latitudinal bands defined above. To highlight seasonal changes, we computed the average for the months of December-January-February (DJF), March-April-May (MAM), June-July-August (JJA) and September-October-November (SON). Ozone loss trends due to VSL^{Br} between 2000 and 2100 were calculated on the basis of the least squares linear trends, while the trend errors were estimated as twice the statistical deviation stemming from the least squares fit.

To provide a basic evaluation of the model performance, the modelled results of the TOC and the inorganic halogen abundances were compared with the following selected observation data sets:

I) The Microwave Limb Sounder (MLS) observations of the annual mean volume mixing ratio of HCl + ClO (Waters et al., 2006; Livesey et al., 2018), which provides a lower limit of the Cl_y abundance in the stratosphere from 2005 to 2015.

II) The Br_y trend reported in the latest WMO Ozone Assessment Reports (WMO, 2014, 2018), which shows changes in total Br_y between 1991 and 2012 derived from stratospheric BrO observations by balloon-borne (Dorf et al., 2006) and ground-based UV-visible (at Harestua (60° N) and Lauder (45° S)) measurements (Hendrick et al., 2007, 2008).

III) The Solar Backscatter Ultraviolet (SBUV-MOD) merged total ozone column data set (Frith et al., 2014, 2017) from 1980 to 2015.

An important point to highlight about the SBUV-MOD data set (and its uncertainties), is that it was constructed from ozone profiles measured by individual SBUV instruments and retrieved using the Version 8.6 algorithm (Bhartia et al., 2013; Frith et al., 2014, 2017). To maintain consistency over the entire time series, the individual instrument records were analysed with respect to each other and absolute calibration adjustments were applied as needed based on comparison of radiance measurements during periods of instrument overlap (DeLand et al., 2012;

Weber et al., 2013). During the overlap periods, the records of the involved SBUV instruments were combined using a simple average. Frith et al. (2014) have estimated the potential errors in the SBUV-MOD data set through Monte Carlo model simulations, taking into account the range of offsets and drifts observed during the overlap periods between individual SBUV instruments and between SBUV and Dobson ground-based measurements. The authors also assessed the extent to which these potential errors might affect the long-term variability of ozone in a multiple-regression model. See Frith et al. (2014) for a detailed description of the data used and their associated uncertainties in the SBUV-MOD.

3. Results and Discussion

3.1 Contribution of LL^{Cl}, LL^{Br} and VSL^{Br} to stratospheric inorganic halogen loading

The evolution (1960−2100) of the modelled annual mean abundances of inorganic chlorine (Cl_y) and bromine (Br_y), as well as the VSL^{Br} sources, in the global upper stratosphere (3.5 hPa) and lower stratosphere (50 hPa) at mid-latitudes and tropics, are shown in Fig.1. In addition, Figure 1 includes global Br_y trends reported in recent WMO reports (WMO, 2014 and 2018) and the MLS observations (HCl + ClO). The values of bias, normalized mean bias (NMB) and normalized mean error (NME) to evaluate the agreement between the modelled Cl_y and observations for each of the regions under study, are shown in Table S1. Clearly, the temporal evolution of Cl_y^{LL} and Bry^{LL} shows a pronounced peak at the end of the 20th century and beginning of the 21st century, respectively, after which the abundance of both halogens decline. Within the A1 halogen emission scenario considered in this work, the Cl_y^{LL} abundance in our model returns to its past 1980 levels just before ~2060 in the global upper stratosphere, whereas the prevailing Bry^{LL} abundance for year 1980 are not recovered even by the end of the 21st century (see Fig 1a). In comparison, the evolution of Br_y^{VSL} abundances remains constant over time, resulting in an additional and time-independent fixed contribution of ~5 ppt total bromine injection, which leads to maximum global-upper stratosphere Br_y^{LL+VSL} abundances of up to ~ 20.5 ppt at the beginning of the 21st century. This is in agreement with previous studies performed only for present-day conditions (Fernandez et al., 2014). Furthermore, note that the modelled global Br_y^{LL+VSL} abundances are in good agreement with the observations within reported errors, highlighting the importance of considering the additional contribution from VSL^{Br} to determine the overall evolution of stratospheric ozone during the 21st century.

In the lower stratosphere at 50 hPa, Br_y^{LL} abundances returns to 1980 levels before ~2080 and ~2050 for the mid-latitudes and tropics, respectively, while the Cl_y^{LL} return date remains unaltered (see Fig. 1b–d). Furthermore, the contribution from VSL^{Br} to mid-latitude total inorganic bromine also reaches ~5 ppt throughout the modelled period, while in the tropics, prevails a small carbon-bonded organic fraction that has not been converted to the reactive inorganic form. Falk et al. (2017) showed an increase of VSL^{Br} of about 0.5 ppt in the tropical lowermost stratosphere by the end of the century compared to present-day, under the RCP6.0 scenario and assuming constant VSL^{Br} fluxes, following scenario five of Warwick et al. (2006). This increase in the stratospheric VSL^{Br} attributed to enhanced vertical transport in the tropics, is counteracted by a decrease of the Br_y^{VSL} injected into the stratosphere, so that the total stratospheric VSL-bromine remains unchanged between the two periods. In this work, the stratospheric injection of VSL^{Br} and Br_y^{VSL} between 2000 and 2100 remain unchanged. Based on the limited observational data, it is uncertain to draw a conclusive statement whether any trend in the stratospheric injection of

organic and inorganic VSL-bromine would be expected. Nevertheless, our stratospheric injection of VSL^{Br} (~2 ppt) and Br_y^{VSL} (~3 ppt) at present-day is in perfect accordance with that reported in the latest WMO (2018). Further studies are needed to evaluate the uncertain evolution of the stratospheric injection of organic and inorganic species from VSL^{Br} sources throughout the 21st century.

The modelled inorganic chlorine abundance shows a good agreement with the (HCl + ClO) MLS observations for the 2005-2015 period, mainly in the upper stratosphere where most chlorine has already been photochemically converted to Cl_y^{LL}. For example, the normal mean error of the comparison between modelled Cl_y^{LL} abundances and MLS observations is about 3.5 % and 19 % at 50 hPa for the mid-latitudes and tropics respectively, while the NME is about 2% for the global mean at 3.5 hPa (see Table S1). This relatively good agreement between the model and MLS observation occurs even without consideration of the recent contribution of anthropogenic VSL^{Cl} sources (i.e., Hossaini et al., 2015b, 2017). Moreover, the inter-annual variation of MLS observations at 50 hPa occurs mainly due to the chlorine heterogeneous reactivation, which can be influenced by the polar vortex dynamics at the mid-latitudes (Dhomse et al. 2018). Note that although in the Section 3.4 we processed output at 120 hPa in the mid-latitude lowermost stratosphere, we did not compare Cl_y^{LL} at this altitude level. This is because below of 50 hPa, the fractional conversion of organic chlorine to Cl_y^{LL} is very small and thus the inferred HCl + ClO MLS data has a very large uncertainty that prevents a reliable model-observation inter-comparison (Santee et al. 2011).

The stratospheric Bry^{VSL} injection remains constant during the whole modelled period, representing ~25 % of Br_y^{LL+VSL} in the global-upper stratosphere for year 2000, and increasing up to ~40 % by the end of the 21st century. These results are in agreement with those reported by Fernandez et al. (2017). Due to the much shorter lifetimes of VSL^{Br} with respect to LL^{Br}, the percentage contributions is larger in the lower stratosphere. For example, the Br_y^{VSL} relative contribution to Br_y^{LL+VSL} for year 2000 at 50 hPa represents ~30 % and ~45 % for the mid-latitudes and tropics, respectively. Furthermore, within the mid-latitudes, Br_y^{VSL} represents up to 45 % of Br_y^{LL+VSL} both at the end of the 21st century and in the years prior to 1980, while in the tropics, Br_y^{VSL} represents up to 65 % for these time periods. Consequently, these changes in the relative contribution of VSL^{Br} to total inorganic bromine over time, region and altitude under different inorganic chlorine abundances, lead to relatively different ozone losses within those regions and altitude regimes, as described in detail below.

Figure 2 shows the annual zonal mean distribution of inorganic chlorine and bromine abundances, as well as the corresponding ClO_x/Cl_y and BrO_x/Br_y percentage ratios (black contour lines) for present-day. Note that the ClO_x/Cl_y and BrO_x/Br_y ratios reflect the changes in the contribution of the active chlorine (ClO_x=ClO + Cl + HOCl + $2Cl_2O_2$ + OClO + $2Cl_2$) and bromine (BrO_x= BrO + Br) fractions relative to their total inorganic abundances. Equivalent results are presented for the end of the 21st century period in the Supporting Information (see Fig. S1). In the lowermost stratosphere, the available inorganic fraction of both chlorine and bromine rapidly increase with altitude as halogen atoms are released by the photolysis and oxidation from all LL^{Cl}, LL^{Br} and VSL^{Br} species. In contrast, within the upper stratosphere no major changes on inorganic halogen abundances are observed since the conversion from their organic sources is nearly complete. Although our model shows a symmetric hemispheric distribution in stratospheric Cl_y and Br_y abundances, there is a marked difference in the ClO_x/Cl_y ratio. In fact, the experiments capture a local increase in the ClO_x/Cl_y ratio at 15ºN and ~100 hPa, as a result of a large increase in the Cl_y species heterogeneous reactivation due to the enhanced vertical transport during the Indian summer monsoon (Solomon et al., 2016b). In the same line, the higher $ClOx/Cl_y$ values modelled in the SH-ML lowermost stratosphere compared

to NH-ML are mainly due to the enhancement in the chlorine heterogeneous reactivation processes on ice-crystals (i.e., HCl and $ClONO_2$ reactivation) (Santee et al., 2011; Solomon et al., 1999, and references therein), influenced mainly by the proximity of the Antarctic polar vortex edge and the lower temperatures prevailing at high and mid-latitudes of the southern hemisphere (see Fig. S2). Additionally, the favourable conditions for isentropic exchange of young subtropical air with extremely old winter polar vortex air masses within the SH-ML (Spang et al. 2015; Rolf et al. 2015) could drive an additional chlorine heterogeneous reactivation and thus enhance hemispheric asymmetry. Moreover, the increase in the ClO_x abundance and ClO_x/Cl_y ratio is highest during winter and spring for both SH-ML and NH-ML, consistent with the seasonal changes of the lowermost stratospheric temperatures that affect chlorine reactivation on ice-crystals (see Fig. S3). In contrast, a symmetric hemispheric distribution of BrO_x/Br_y ratio is modelled in the mid-latitude lowermost stratosphere, associated with bromine heterogeneous reactivation on sulphate aerosols instead of ice-crystals (i.e., HBr and $BrONO_2$ reactivation) (Solomon et al., 1999, and references therein), which show neither any hemispheric asymmetry nor seasonal changes in the reactivation processes (see Fig. S4). Thus, even when the inclusion of VSL^{Br} sources increase the total stratospheric Br_y abundance and therefore its active fraction (BrO_x), the BrO_x/Br_y ratio remains unchanged in the stratosphere during the whole modelled period (see Figs. 2b,c and S1b,c), highlighting that this ratio is nearly independent of the total inorganic bromine abundance.

3.2 Impact of VSL^{Br} on the seasonal evolution of total ozone column (TOC)

The temporal evolution (1960–2100) of the modelled annual mean TOC at the mid-latitudes and tropics, along with SBUV-MOD TOC observations, is illustrated in Fig. 3. Equivalent results for the temporal evolution of the individual simulations of each experiment, are shown in Fig. S5. Table 1 shows the annual and seasonal mean values of the absolute and relative TOC differences (ΔTOC) between the experiments for the present-day and the end of the 21st century periods, as well as the ΔTOC trends (% dec^{-1}) over the century. In addition, Table S2 shows the values of bias, normalized mean bias (NMB) and normalized mean error (NME) to evaluate the agreement between the modelled TOC and observations for each of the regions under study. Based on the comparison of the TOC results over the different latitudinal bands, the following features can be described:

I) The constant emission of biogenic VSL^{Br} sources, introduces a continuous reduction in TOC that exceeds the mean ensemble variability between the experiments (see Fig. S5). Moreover, the inclusion of VSL^{Br} sources improves the overall agreement between the model and observations with a reduction of 1 and 0.9 % in NME for the SH-ML and NH-ML, respectively (see Table S2). However, the inclusion of VSL^{Br} sources leads to a slight increase of 0.2 % in NME for the tropics. Note is that the statistical analysis presented in Table S2 does not take into account the uncertainties that may arise from the merging of the individual SBUV instruments in the SBUV-MOD data set (see Section 2).

II) Within the mid-latitudes, the additional ozone loss due to VSL^{Br} peaks during the present-day period, coinciding with the temporal location of the minimum TOC for both experiments and reaching a ΔTOC^{2000} of approximately −8 DU (~ −2.5 %) and −5.5 DU (~ −1.6 %) for the SH-ML and NH-ML, respectively (See Table 1). Moreover, VSL^{Br} impacts on TOC by the end of the 21st century are ~50% lower than the values found for the present-day, which is in line with the projected ΔTOC trends of 0.15 and 0.10 % dec^{-1} for the SH-ML and NH-ML, respectively.

III) Within the tropics, the inclusion of VSL^{Br} leads to small impacts on TOC compared to impacts observed at mid-latitudes. The TOC differences due to VSL^{Br} are close to −1.5 DU (< −1 %) during practically the entire modelled period, with a maximum ΔTOC^{2000} reaching − 2.1 DU (< −1 %). This is in line with a projected ΔTOC trend of 0.03 % dec^{-1}. Moreover, even though the VSL^{Br} slightly worsens the agreement between the modelled TOC^{LL} and observations, the minimum TOC^{LL+VSL} is shifted ~5 years earlier compared to TOC^{LL} (i.e. towards where the inorganic chlorine peak is located in year 1995), in agreement with observations.

IV) Overall, our model results show a much higher ozone depletion due to the VSL^{Br} within the southern and northern mid-latitudes compared to the tropics.

Our results of the mid-latitude ΔTOC due to VSL^{Br} lie within the lower range of previous modelling studies over the 1960–2005 (Sinnhuber and Meul, 2015) and 1980–2005 (Feng et al., 2007) periods. The lower impacts modelled in this work during recent past are expected, as for example the detailed treatment of VSL^{Br} sources in Sinnhuber and Meul (2015) results in an additional Br_y^{VSL} injection of 6 ppt Br_y. While in Feng et al. (2007), the model configurations included, in addition to a VSL tracer, the direct supply of tropospheric Br_y as a lower condition. Furthermore, our results are in accord with the future projection trends in Falk et al. (2017), although their analysis on annual mean ozone loss due to VSL^{Br} only focused on the late 21st century (2075–2100).

Figure 4 shows the temporal evolution (1960–2100) of the annual and seasonal ΔTOC between the experiments for the SH-ML, tropics and NH-ML. In addition, an analysis of ΔTOC as a function of latitude for present-day and the end of the 21st century periods is shown in Fig. 5. The inclusion of VSL^{Br} leads to a continuous reduction of TOC at all latitudes, with a larger ozone destruction efficiency moving from the tropics to the high-latitudes. Moreover, note that when comparing the seasonal relative ΔTOC between both periods, a statistically significant difference (here defined as $p < 0.05$) is only observed at the mid-latitudes, as shown by the horizontal lines at the bottom of Fig. 5d. This highlights that the VSL^{Br}-driven ozone depletion efficiency changes significantly over the century, even though the contribution from VSL^{Br} sources to bromine stratospheric injection remains constant. Since gas-phase and heterogeneous inter-halogen reactions involving both bromine and chlorine play a fundamental role in the stratospheric ozone loss (McElroy et al., 1986; Solomon et al., 1999; Salawitch et al., 2005), the VSL-bromine efficiency in ozone depletion is primarily linked to the background inorganic halogen abundance, which shows a continuous decline in the course of the 21st century contemplated in the A1 halogen emission scenario considered in this work. This is in line with the findings of Yang et al. (2014). Therefore, an additional stratospheric chlorine and bromine load from natural or anthropogenic substances not regulated by the Montreal Protocol, will induce an increase in the VSL^{Br} impacts modelled in this work on projected ozone loss trends throughout the current century.

Largest mid-latitude TOC differences between experiments occur during spring −when the maximum seasonal TOC levels are found− followed by the winter. Maximum springtime ΔTOC^{2000} reaches −10 DU (~ −3 %) and −7.7 DU (~ −2 %) for the SH-ML and NH-ML, respectively (see Table 1 and Fig. 4). In contrast, during summer and autumn, the maximum ΔTOC^{2000} remain below −6.8 (~ −2.4 %) and −4 DU (~−4.1 %) for the SH-ML and NH-ML, respectively. This is in line with the ozone loss mediated by VSL^{Br} within the southern polar cap reported by Fernandez et al. (2017), whom showed a maximum ozone depletion of up to −15 DU (~ −14 % of TOC) during the October months at the beginning of the century. Moreover, as mentioned above, the projected seasonal VSL^{Br} impact on TOC significantly decreases towards the end of the century, with springtime ΔTOC trends of up to 0.20

and 0.14 % dec^{-1} for the SH-ML and NH-ML, respectively (see Table 1). In comparison, the projected ΔTOC trends for summer and autumn reach approximately 0.10 % dec^{-1} at mid-latitudes. Note also that the changes in the magnitudes of these seasonal ΔTOC trends are mainly attributed to a marked seasonal difference of ozone loss mediated by VSL^{Br} during the period of highest background halogen abundance (i.e. present-day). These seasonal differences are reduced towards the end of the 21st century, due to the declining of the long-lived inorganic halogens abundance.

Within the tropics, no significant changes in the TOC loss due to VSL^{Br} is projected, though the model captures a slightly major TOC depletion during the 1990s. Therefore, the VSL^{Br}-driven ozone depletion is less sensitive to background halogen abundances, introducing an almost constant impact that is in line with its fixed emissions considered throughout the whole modelled period.

3.3 VSL^{Br} impact on ozone vertical distributions.

Timeline analysis of the annual mean stratospheric ozone difference between the experiments as a function of altitude within the mid-latitudes and tropics, is presented in Fig. 6. The inclusion of VSL^{Br} produces a reduction in ozone concentrations (i.e., $O_3(z)$ number densities) throughout most of the stratosphere during the whole modelled period. Largest $O_3(z)$ reductions occur during the present-day period at the mid-latitude lowermost stratosphere, reaching ozone differences ($\Delta O_3(z)$) of up to −8 % (−0.25 x 10^{12} molecule cm^{-3}) and −5 % (−0.14 x 10^{12} molecule cm^{-3}) for the SH-ML and NH-ML, respectively. Above 50 hPa (~20 km), the $\Delta O_3(z)$ are practically constant at around −1% for all latitudes, which are linked to the lesser role played by VSL-bromine compared to catalytic ozone losses by hydrogen (HO_x= OH+HO_2) and nitrogen (NO_x= NO+NO_2) oxides, as well as by long-lived reactive halogens (Brasseur and Solomon, 2005; Salawitch et al., 2005; Müller, 2012).

Our modelled $\Delta O_3(z)$ latitudinal distribution is in agreement with those reported by Sinhuber and Meul et al. (2015) during the 1980–2005 period, with larger percentage ozone loss deepening around the mid−latitudes tropopause. In addition, the $O_3(z)$ reduction due to VSL^{Br} in the mid-latitudes lowermost stratosphere is about 50% smaller by the end of the 21st century period compared to the present-day period (see Figs. 6d and 6e). This is in line with projected local $\Delta O_3(z)$ trends of up to 1 and 0.5 % dec^{-1} in the SH-ML and NH-ML, respectively (see Fig. 6f). Largest $O_3(z)$ reductions are located precisely at the same altitudes and latitudes where the ClO_x/Cly ratio peak is modelled within the SH-ML lowermost stratosphere (see Fig. 2), which explains the hemispheric asymmetry in the VSL^{Br} impacts. This highlights that the enhancement in local ozone depletion mediated by VSL^{Br} is largest under a context of highest background active chlorine abundance, since it provides an additional partner for chlorine species involved in the ozone depleting inter−halogen chemical reactions (e.g. ClO_x–BrO_{x-Loss}, see Section 3.4). These results are in agreement with Yang et al. (2014), who determined that VSL^{Br} has a significantly larger ozone impact under a high stratospheric chlorine background than under a low chlorine background, using a set of time-slice sensitivity simulations with a variable and speculative VSL^{Br} contribution on different background stratospheric Cl_y abundances.

Figure 7 shows the seasonal zonal mean distribution of the $\Delta O_3(z)$ during the present-day period. The corresponding $\Delta O_3(z)$ trends (% dec^{-1}) over the century, are shown in Fig. S6. The largest contributions to the annual mean ozone loss in the mid-latitude lowermost stratosphere correspond to spring, followed by the preceding winter and the posterior summer on each hemisphere, with springtime $\Delta O_3(z)$ reaching up to −10 % and −7 % for the SH-ML and

NH-ML, respectively (see Fig. 7b,d). This seasonal enhancement in VSL^{Br}-mediated local ozone depletion is influenced by the seasonal changes of the chlorine heterogeneous reactivation processes on lowermost stratospheric ice-crystals, since the main bromine heterogeneous reactivation processes occurs on sulphate aerosols, and therefore, lack of seasonal changes (see Figs. S3 and S4). Consequently, since the seasonal changes in the ozone losses are maximized during the present−day period, the largest local $\Delta O_3(z)$ trends are also projected for spring and winter, with springtime $\Delta O_3(z)$ trends reaching up to 1.6 and 0.7 % dec^{-1} for the SH-ML and NH-ML, respectively (see Fig. S6b,d).

Compared to the annual mean, springtime absolute $O_3(z)$ reductions along mid-latitudes are deepened over the first ~ 5 km above the tropopause during the present-day period. Whereas during summer and autumn, these reductions are located at higher altitudes (between 2 and 5 km above the tropopause) and over a narrower geographic area, mainly in the NH-ML. Therefore, the VSL-bromine introduces seasonal changes not only in the overall $O_3(z)$ reduction, but also in the vertical $O_3(z)$ distribution. Moreover, since seasonal VSL^{Br} impacts persist until the end of the century, they could lead to significantly different seasonal perturbations on the radiative effects mediated by ozone. Future studies are needed to explore the potential VSL^{Br}-mediated seasonal effects on atmosphere's radiative balance.

Near the tropical tropopause, the $O_3(z)$ reductions due to VSL^{Br} are practically constant during the whole modelled period, with $\Delta O_3(z)$ of approximately −2% ($-0.06\ 10^{12}$ molecule cm^{-3}) at 50 hPa (see Fig. 6b). Even with an increase in the contribution of Bry^{VSL} to Br_y^{LL+VSL} of up to 65 % by the end of century −due to the implementation of the Montreal Protocol (WMO, 2014, 2018) and the fixed stratospheric Br_y^{VSL} injection– $\Delta O_3(z)$ changes in the tropical lowermost stratosphere are not significant over the century (see Fig. 6f). This is in line with the modelled impacts on TOC. In contrast, within mid-latitudes, the seasonal VSL^{Br} impacts on ozone significantly decrease over the century between 50 hPa and 300 hPa (see Figs. 6f and S6a–d), even though the percentage contribution from Bry^{VSL} to Br_y^{LL+VSL} increases towards the end of the century. Moreover, the projected seasonal and annual $\Delta O_3(z)$ trends peak precisely at the same altitudes where the modelled relative $\Delta O_3(z)$ are significant (see Figs. 6f and S6a–d). These result highlights the clear dependence of VSL^{Br} impacts with the temporal evolution of background halogen abundances and the halogens heterogeneous reactivation processes, which in turn depend on temperature as well as the formation and distributions of ice-crystal and stratospheric sulphate aerosol surfaces. In fact, the projected impacts on the ozone vertical distribution at the end of the century are similar to those prevailing before 1980 for both SH-ML and NH-ML, since the background halogen abundances are similar between these periods. Thus, potential future changes in the lowermost stratospheric temperature (i.e. influencing the ice-crystal formation), geoengineering of climate via injection of stratospheric sulphate, as well as the formation and distribution of stratospheric aerosol (e.g. future volcanic eruptions) will directly influence the processes of halogen heterogeneous reactivation and consequently the VSL^{Br}-driven ozone depletion efficiency (Tilmes et al., 2008, 2012; Banerjee et al., 2016; Klobas et al., 2017; Heckendorn et al., 2009).

3. 4 Changes in the long-term seasonal evolution of Halogen-driven ozone loss rate due to VSL^{Br}

In order to determine the drivers controlling the VSL^{Br}-driven seasonal impact on ozone in the lowermost stratosphere at mid-latitudes and tropics, we compute the odd oxygen chemical loss from the each ozone-depleting families, considering the independent contributions of oxygen (O_{x-Loss}), hydrogen (HO_{x-Loss}), nitrogen (NO_{x-Loss}),

and halogen ($Halog_{x-Loss}$) (Brasseur and Solomon, 2005; Saiz–Lopez et al., 2014). Moreover, we discriminate the individual contribution of pure bromine (BrO_{x-Loss}) and chlorine (ClO_{x-Loss}) cycles and inter-halogen (ClO_x-BrO_{x-Loss}) cycle to the halogen family ($Halog_{x-Loss} = BrO_{x-Loss} + ClO_{x-Loss} + ClO_x-BrO_{x-Loss}$). The odd oxygen loss rates equations for the ozone-depleting families considered in this work are presented in Table S3.

Figure 8, shows the temporal evolution of the annual percentage contribution of each ozone-depleting family to total ozone loss rate in the SH–ML lowermost stratosphere (~120 hPa) for both experiments, as well as the seasonal evolution of HO_{x-Loss} and $Halog_{x-Loss}$ contributions in each experiment. The corresponding figures for the lowermost stratosphere at the NH–ML (~120 hPa) and tropics (~50 hPa), are shown in Figs. S7 and S8, respectively. $Halog_{-Loss}$ represents the second most important contribution to total ozone loss rate after HO_{x-Loss} (~ 80 %) at the mid-latitude in both experiment (see Figs. 8a and S7a), while within the tropics it represents the third family after HO_{x-Loss} and NO_{x-Loss} (see Fig. S8a). This partially explains the smaller modelled VSL-bromine impact on ozone within the tropics, as $Halog_{x-Loss}^{LL+VSL}$ represents at most 10% of the total ozone destruction over this region. Moreover, the enhancement in the $Halog_{x-Loss}^{LL+VSL}$ contribution with respect to $Halog_{x-Loss}^{LL}$ by including VSL^{Br}, is mostly compensated by a decrease in the HO_{x-Loss}^{LL+VSL} contribution within the mid-latitudes. For example, during the present-day, $Halog_{x-Loss}^{LL+VSL}$ shows an increase of ~7 % with respect to $Halog_{x-Loss}^{LL}$ within the SH-ML, which is compensated by a reduction of ~6 % in HO_{x-Loss}^{LL+VSL}. In particular, the interaction between different catalytic ozone-depleting cycles involving OH and halogen radicals, as well as the influence of reactive halogens in altering the OH/HO_2 ratio, have been described elsewhere (Bloss et al., 2005; Saiz-Lopez and von Glasow, 2012).

Even though the additional seasonal ozone depletion due to VSL^{Br} peaks during spring followed by winter at the mid-latitudes, the largest $Halog_{x-Loss}$ contribution to the total ozone loss rate occurs during winter in both experiments, presenting a much smaller contribution during the rest of the year (see Figs. 8b,c and S7b,c). Indeed, this marked seasonal behaviour prevails both, during boreal winter in the NH-ML and during the austral winter at the SH-ML. This is explained by considering the strong seasonal increase in the active chlorine abundance (i.e. driven by the heterogeneous reactivation on ice-crystals), as well as the winter decline of HO_x abundance (i.e driven by the decrease in solar radiation with respect to summertime). In fact, the enhancement in the $Halog_{x-Loss}^{LL+VSL}$ contribution due to VSL^{Br}, makes it the dominant ozone depleting family during winter between 1985 and 2020 within the SH–ML, surpassing in importance the role played by the otherwise dominant HO_{x-Loss}. In contrast, no seasonal variability of $Halog_{x-Loss}$ contribution is modelled within the tropics in both experiments (see Fig. S8b,c), and thus the seasonal VSL^{Br} impact on ozone remains approximately constant during the whole modelled period around the annual mean.

Figure 9 shows the long-term evolution of the percentage contribution of BrO_{x-Loss}, ClO_{x-Loss} and $ClO_x–BrO_{x-Loss}$ to the $Halog_{x-Loss}$ as a function of months and years in the SH-ML lowermost stratosphere (120 hPa) for both experiments. Equivalent results are presented for the NH-ML and tropics in Figs. S9 and S10, respectively. For any fixed year in both experiments, the BrO_{x-Loss} contribution peaks during late summer and early autumn, while its minimum contribution occurs during the austral winter. In contrast, both the ClO_{x-Loss} and $ClO_x–BrO_{x-Loss}$ reach their maximum contribution during winter and early spring. Consequently, the inclusion of VSL^{Br} increases the BrO_{x-Loss}^{LL+VSL} contribution in all seasons, while also increasing the $ClO_x–BrO_{x-Loss}^{LL+VSL}$ contribution mainly in winter. This is at the expense of a decrease in the ClO_{x-Loss}^{LL+VSL} contribution. In addition, the wintertime $ClO_x - BrO_{x-Loss}^{LL+VSL}$ contribution reaches up to 50 % between 1990 and 2020, decreasing towards the end of the century as Cl_y^{LL} and

Br_y^{LL} abundances decrease within the A1 emission scenario. Both, the decrease of ClO_{x-Loss}^{LL+VSL} and ClO_x–BrO_{x-Loss}^{LL+VSL} over time is offset by an increase in the BrO_{x-Loss}^{LL+VSL} contribution. Accordingly, the inclusion of VSL^{Br} produces similar changes in the evolution of the contributions of each of the cycles that compose $Halog_{x-Loss}$ at the NH-ML, although the seasonal BrO_{x-Loss} contribution is greater in both experiments compared to the SH-ML during the entire modelled period (see Fig. S9).

In summary, the $Halog_{x-Loss}^{LL+VSL}$ contribution to total ozone loss rate in summer and autumn is almost entirely dominated by BrO_{x-Loss}^{LL+VSL}. While in the winter months, when seasonal $Halog_{x-Loss}^{LL+VSL}$ contribution to total ozone loss rate is comparatively higher, a transition from the ClO_x– BrO_{x-Loss}^{LL+VSL} contribution (~50 %) at the beginning of the century towards BrO_{x-Loss}^{LL+VSL} at the end of the century is modelled. Thus, the halogen-driven ozone losses projected towards the end of the 21st century are mostly dominated by BrO_{x-Loss}, leading to a less marked seasonal VSL^{Br} impact in accordance with the modelled results on both the ozone vertical distribution and the TOC. On the other hand, within the tropics, BrO_{x-Loss}^{LL+VSL} dominates the seasonal $Halog_{x-Loss}^{LL+VSL}$ contribution for practically the entire modelled period (see Fig. S10), while ClO_{x-Loss}^{LL+VSL} represents a maximum contribution of up to ~35% during the end 20th century. The seasonal increase from BrO_{x-Loss}^{LL} to BrO_{x-Loss}^{LL+VSL} by including VSL^{Br} is well marked, which is practically offset by a reduction in the ClO_{x-Loss}^{LL+VSL} contribution. Furthermore, unlike mid-latitudes, ClO_x–BrO_{x-Loss}^{LL+VSL} has a lower contribution to the tropical $Halog_{x-Loss}^{LL+VSL}$, showing that the VSL^{Br}-driven topical ozone loss is independent of changes in the background halogen abundance throughout the modelled period.

4 Conclusions

This study has explored the impact of VSL^{Br} substances on the temporal evolution of stratospheric ozone both in the late 20th century and in the course of the 21st century at the mid-latitudes and tropics. The analysis compares two independent experiments, one of which considers only the anthropogenic LL^{Cl} and LL^{Br} sources contributions, while the other considers−in addition to long-lived sources− the contributions of VSL^{Br} oceanic sources. We have evaluated annual and seasonal mean changes on the stratospheric ozone vertical distribution and TOC, as well as examined the projected ozone depletion (ΔO_3 and ΔTOC) trends over the century, under a scenario where both the relative contribution of VSL^{Br} to total inorganic bromine and the background inorganic chlorine abundances shift towards the future. Finally, we have also assessed the long-term seasonal contribution changes of the halogen-mediated ozone losses ($Halog_{x-Loss}$) due to VSL-bromine focused on the lowermost stratosphere, distinguishing the role of pure (BrO_{x-Loss}, ClO_{x-Loss}) and inter-halogen (ClO_x–BrO_{x-Loss}) cycles that compose $Halog_{x-Loss}$. The results presented here highlight the importance of considering natural sources of halocarbons to determine the overall evolution of stratospheric ozone in the tropics and mid-latitudes during the 21st century.

Our analysis shows that the inclusion of VSL^{Br} results in a realistic stratospheric bromine loading that improves the agreement between the model and observations of TOC at the mid-latitudes, highlighting the need to consider these additional natural emissions to determine the overall evolution of ozone during the 21st century. Our results are in accordance with previous modelling studies that included natural bromocarbons and explored stratospheric ozone in the recent past (Salawitch et al., 2005; Feng et al., 2007; Sinhuber et al., 2015), as well as by the end of the 21st century (Falk et al., 2017). However, unlike these previous works, we have explored the seasonal ozone depletion arising from VSL^{Br} with respect to the background stratospheric LL^{Cl} and LL^{Br} abundances between the 1960-2100 period.

Within the mid-latitudes, the VSL^{Br} introduces a continuous reduction on TOC during the entire modelled period, with the largest TOC depletion occurring during the period of highest background halogen abundance (ΔTOC^{2000}= −8 DU (−2.5 %) for SH-ML and −5.5 DU (−1.6 %) for NH-ML). In turn, a significant decrease of the impact towards the end of the 21st century at the mid-latitudes is projected, with ΔTOC trends of 0.15 and 0.10 % dec^{-1} for SH-ML and NH-ML, respectively. Even though the contribution of VSL-bromine to total stratospheric bromine reaches almost 50% by the end 21st of the century, our simulations show a statistically significant smaller VSL^{Br} impact on lowermost stratospheric ozone as we move into the future. This result highlights that VSL^{Br}-driven ozone loss is closely linked to the temporal evolution of LL^{Cl} and LL^{Br} abundances regulated by the Montreal Protocol, as suggested by Yang et al. (2014). In the same line, Hossaini et al. (2015a) demonstrated that the chlorine load in the lowermost stratosphere has increased as a consequence of a recent and ongoing growth in emissions from anthropogenic VSL^{Cl} sources (mainly CH_2Cl_2) not controlled by the Montreal Protocol. If this VSL^{Cl} emissions trend continues into the future, additional studies will be required to quantify the increase in VSL-bromine impact modelled in this work on the projected ozone loss trends over the century, considering the additional inorganic chlorine from VSL^{Cl}.

Largest TOC depletion associated with VSL^{Br} corresponds to the spring months followed by winter, with maximum springtime ΔTOC^{2000} reaching −10 DU (~ −3 %) and −7.7 DU (~ −2 %) for SH-ML and NH-ML, respectively. We find that the inclusion of VSL^{Br} leads to seasonal changes in both local $O_3(z)$ reduction and its vertical $\Delta O_3(z)$ distribution within the lowermost stratosphere, which could result in different seasonal perturbations on the radiative effects mediated by ozone. This seasonal enhancement in the VSL^{Br}-mediated local ozone loss is strongly influenced by the seasonal changes in chlorine heterogeneous reactivation processes on ice crystals (mainly by the $ClONO_2$ and HCl recycling). In fact, the modelled additional increase in the chlorine heterogeneous reactivation efficiency in the lowermost stratosphere of SH-ML compared to NH-ML, leads to hemispheric asymmetry in the VSL^{Br}-driven ozone reductions.

Even though the additional seasonal ozone depletion due to VSL^{Br} peaks during spring followed by winter, the largest $Halog_{x-Loss}^{LL+VSL}$ contribution to total ozone loss rate occurs during winter, with a much smaller contribution during all other seasons. In fact, the wintertime $Halog_{x-Loss}^{LL+VSL}$ contribution dominantes the total ozone loss rate between 1985 and 2020 in the SH-ML lowermost stratosphere, with a ClO_x–BrO_{x-Loss}^{LL+VSL} contribution to $Halog_{x-Loss}^{LL+VSL}$ reaching up to 50%. Due to the expected decrease in the LL^{Cl} and LL^{Br} abundances, a transition from ClO_x–BrO_{x-Loss}^{LL+VSL} to BrO_{x-Loss} during the course of the 21st century is projected, leading to a less marked seasonal VSL^{Br} impact towards the end of the century.

Within the tropics, although our model captures a slightly greater TOC depletion associated with VSL^{Br} during the 1990s, no significant change is projected by the end of the 21st century. $Halog_{-Loss}$ represents the third family in the contribution to total ozone loss rate after the HO_{x-Loss} and NO_{x-Loss} in the tropical lowermost stratosphere, with an almost constant seasonal contribution throughout the modelled period. BrO_{x-Loss}^{LL+VSL} practically dominates the contribution to $Halog_{x-Loss}^{LL+VSL}$, with a maximum ClO_x–BrO_{x-Loss}^{LL+VSL} contribution of up to ~30% by the end of the 20th century, reflecting the low sensitivity of VSL-bromine to background halogen abundances to drive the stratospheric ozone depletion.

5 Data availability.

Computing resources, support and data storage are provided and maintained by the Computational and Information System Laboratory from the National Center of Atmospheric Research (CISL, 2017). The code of the CAM-Chem model can be downloaded from the site (https://www2.acom.ucar.edu/gcm/cam-chem). Data that support the finding of this study can be downloaded from the AC2 webpage (https://ac2.iqfr.csic.es/en/publications).

6 Author Contributions

R.P.F and A.S-L. designed the experiments. R.P.F and J.A.B configured and run all the simulations. J.A.B processed the result of all simulations, led the manuscript and prepared the figures. RPF, A.S-L., F.I-S and C.A.C provided additional feedback on geophysical processing and representation. All co-authors were involved in the discussion and iterations of the manuscript.

7 Competing interests.

The authors declare that they have no conflict of interest.

8 Acknowledgements

This study has been funded by the Agencia Nacional de Promoción Científica y Técnica (ANPCYT PICT-2016-0714, Argentina) and the European Research Council Executive Agency under the European Union´s Horizon 2020 Research and Innovation programme (Project 'ERC-2016-COG 726349 CLIMAHAL'). R.P.F and J.A.B. would like to thanks additional financial support from CONICET, UNCuyo (SeCTyP M032/3853) and UTN (PID 4920-194/2018). A.S-L., C.A.C and F.I-S. are supported by the Consejo Superior de Investigaciones Científicas (CSIC) of Spain. We are very thankful to D. Kinnison for very helpful discussions and suggestions. We thank two anonymous reviewers for their helpful comments that improved this manuscript.

9 References

Anderson, J. G., Wilmouth, D. M., Smith, J. B., and Sayres, D. S.: UV Dosage Levels in Summer: Increased Risk of Ozone Loss from Convectively Injected Water Vapor, Science, 337, 835–839, https://doi.org/10.1126/science.1222978, 2012.

Anderson, J. G., Weisenstein, D. K., Bowman, K. P., Homeyer, C. R., Smith, J. B., Wilmouth, D. M., Sayres, D. S., Klobas, J. E., Leroy, S. S., Dykema, J. A., and Wofsy, S. C.: Stratospheric ozone over the United States in summer linked to observations of convection and temperature via chlorine and bromine catalysis, P. Natl. Acad. Sci. USA, 114, 4905–4913, https://doi.org/10.1073/pnas.1619318114, 2017.

Anderson, J. G. and Clapp, C. E.: Coupling free radical catalysis, climate change, and human health, Phys. Chem. Chem. Phys., 20, 10569–10587, https://doi.org/10.1039/C7CP08331A, 2018.

Abrahamsson, K., Granfors, A., Ahnoff, M., Cuevas, C. A., & Saiz-Lopez, A.: Organic bromine compounds produced in sea ice in Antarctic winter, Nat. Commun., 9, 5291–5302, https://doi.org/10.1038/s41467–018–07062–8, 2018.

Banerjee, A., Maycock, A. C., Archibald, A. T., Abraham, N. L., Telford, P., Braesicke, P., and Pyle, J. A.: Drivers of changes in stratospheric and tropospheric ozone between year 2000 and 2100, Atmos. Chem. Phys., 16, 2727–2746, https://doi.org/10.5194/acp–16–2727–2016, 2016.

Bhartia, P. K., McPeters, R. D., Flynn, L. E., Taylor, S., Kramarova, N. A., Frith, S., Fisher, B., and DeLand, M.: Solar Backscatter UV (SBUV) total ozone and profile algorithm, Atmos. Meas. Tech., 6, 2533–2548, https://doi.org/10.5194/amt-6-2533-2013, 2013.

Bloss, W. J., Lee, J. D., Johnson, G. P., Sommariva, R., Heard, D. E., Saiz-Lopez, A., Plane, J. M. C., McFiggans, G., Coe, H., Flynn, M., Williams, P., Rickard, A. R., and Fleming, Z. L.: Impact of halogen monoxide chemistry upon boundary layer OH and HO_2 concentrations at a coastal site, Geophys. Res. Lett., 32, L06814, https://doi.org/10.1029/2004GL022084, 2005.

Brasseur, G. and Solomon, S.: Aeronomy of the Middle Atmosphere: Chemistry and Physics of the Stratosphere and Mesosphere, 3rd Editio., Springer, Dordrecht, The Netherlands, Chapter 5, 265–442, 2005.

Bregman, B., Wang, P. H., and Lelieveld, J.: Chemical ozone loss in the tropopause region on subvisible ice clouds, calculated with a chemistry-transport model, J. Geophys. Res., 107, 4032, https://doi.org/10.1029/2001JD000761, 2002.

Borrmann, S., Solomon, S., Dye, J. E., and Luo, B. P.: The potential of cirrus clouds for heterogeneous chlorine activation, Geophys. Res. Lett., 23, 2133–2136, https://doi.org/10.1029/96GL01957, 1996.

Borrmann, S., Solomon, S., Avallone, L., Toohey, D., and Baumgardner, D.: On the occurrence of ClO in cirrus clouds and volcanic aerosol in the tropopause region, Geophys. Res. Lett., 24, 2011–2014, https://doi.org/10.1029/97GL02053, 1997.

Carpenter, L. J. and Liss, P. S.: On temperate sources of bromoform and other reactive organic bromine gases, J. Geophy. Res., 105, 20539–20547, https://doi.org/10.1029/2000JD900242, 2000.

Carpenter, L. J., Wevill, D. J., Hopkins, J. R., Dunk, R. M., Jones, C. E., Hornsby, K. E., and McQuaid, J. B.: Bromoform in tropical Atlantic air from 25◦N to 25◦S, Geophys. Res. Lett., 34, L11810, https://doi.org/10.1029/2007GL029893, 2007.

Chipperfield, M. P., Bekki, S., Dhomse, S., Harris, N. R. P., Hassler, B., Hossaini, R., Steinbrecht, W., Thieblemont, R., and Weber, M.: Detecting recovery of the stratospheric ozone layer, Nature, 549, 211–218, https://doi.org/10.1038/nature23681, 2017.

CISL. (2017). Computational and Information Systems Laboratory. Cheyenne: HPE/SGI ICE XA System (NCAR Community Computing), Boulder, CO, USA. Boulder, CO, USA: National Center for Atmospheric Reserach (NCAR). https://doi.org/10.5065/D6RX99HX.

Daniel, J. S., Solomon, S., Portmann, R. W., and Garcia, R. R.: Stratospheric ozone destruction: The importance of bromine relative to chlorine, J. Geophys. Res., 104, 23871, https://doi.org/10.1029/1999JD900381, 1999.

DeLand, M. T., Taylor, S. L., Huang, L. K., and Fisher, B. L.: Calibration of the SBUV version 8.6 ozone data product, Atmos. Meas. Tech., 5, 2951–2967, https://doi.org 10.5194/amt-5-2951-2012, 2012.

Dessler, A. E.: Clouds and water vapor in the Northern Hemisphere summertime stratosphere, J. Geophys. Res., 114, D00H09, https://doi.org/10.1029/2009JD012075, 2009.

Dhomse, S. S., Kinnison, D., Chipperfield, M. P., Salawitch, R. J., Cionni, I., Hegglin, M. I., Abraham, N. L., Akiyoshi, H., Archibald, A. T., Bednarz, E. M.., Bekki, S., Braesicke, P., Butchart, N., Dameris, M., Deushi, M., Frith, S., Hardiman, S. C., Hassler, B., Horowitz, L. W., Hu, R.-M., Jöckel, P., Josse, B., Kirner, O., Kremser, S., Langematz, U., Lewis, J., Marchand, M., Lin, M., Mancini, E., Marécal, V., Michou, M., Morgenstern, O., O'Connor, F. M., Oman, L., Pitari, G., Plummer, D. A., Pyle, J. A., Revell, L. E., Rozanov, E., Schofield, R., Stenke, A., Stone, K., Sudo, K., Tilmes, S., Visioni, D., Yamashita, Y., y Zeng, G.: Estimates of ozone return dates from Chemistry-Climate Model Initiative simulations, Atmos. Chem. Phys., 18, 8409–8438, https://doi.org/10.5194/acp–18–8409–2018, 2018.

Dorf, M., Bösch, H., Butz, A., Camy-Peyret, C., Chipperfield, M. P., Engel, A., Goutail, F., Grunow, K., Hendrick, F., Hrechanyy, S., Naujokat, B., Pommereau, J.-P., Van Roozendael, M., Sioris, C., Stroh, F., Weidner, F., and Pfeilsticker, K.: Balloon-borne stratospheric BrO measurements: comparison with Envisat/SCIAMACHY BrO limb profiles, Atmos. Chem. Phys., 6, 2483–2501, https://doi.org/10.5194/acp–6–2483–2006, 2006.

Douglass, A., Stolarski, R. S., Schoeberl, M. R., Jackman, C. H., Gupta, M. L., Newman, P. A., Nielsen, J. E., and Fleming, E. L.: Relationship of loss, mean age of air and the distribution of CFCs to stratospheric circulation and implications for atmospheric lifetimes, J. Geophys. Res., 113, D14309, https://doi.org/10.1029/2007JD009575, 2008.

Drdla, K. and Müller, R.: Temperature thresholds for chlorine activation and ozone loss in the polar stratosphere, Ann. Geophys., 30, 1055–1073, https://doi.org/10.5194/angeo–30–1055–2012, 2012.

Dvortsov, V. L., Geller, M. A., Solomon, S., Schauffler, S. M., Atlas, E. L., Blake, D. R.: Rethinking reactive halogen budgets in the midlatitude lower stratosphere, Geophys. Res. Lett., 26, 1699–1702. https://doi.org/10.1029/1999GL900309. 1999.

Eyring, V., Cionni, I., Bodeker, G. E., Charlton-Perez, A. J., Kinnison, D. E., Scinocca, J. F., Waugh, D. W., Akiyoshi, H., Bekki, S., Chipperfield, M. P., Dameris, M., Dhomse, S., Frith, S. M., Garny, H., Gettelman, A., Kubin, A., Langematz, U., Mancini, E., Marchand, M., Nakamura, T., Oman, L. D., Pawson, S., Pitari, G., Plummer, D. A., Rozanov, E., Shepherd, T. G., Shibata, K., Tian, W., Braesicke, P., Hardiman, S. C., Lamarque, J. F., Morgenstern, O., Pyle, J. A., Smale, D., and Yamashita, Y.: Multi-model assessment of stratospheric ozone return dates and ozone recovery in CCMVal-2 models, Atmos. Chem. Phys., 10, 9451–9472, https://doi.org/10.5194/acp-10-9451-2010, 2010.

Eyring, V., Lamarque, J.-F., Hess, P., Arfeuille, F., Bowman, K., Chipperfield, M. P., Duncan, B., Fiore, A.,

Gettelman, A., Giorgetta, M. A., Granier, C., Hegglin, M., Kinnison, D., Kunze, M., Langematz, U., Luo, B., Martin, R., Matthes, K., Newman, P. A., Peter, T., Robock, A., Ryerson, T., Saiz-Lopez, A., Salawitch, R., Schultz, M., Shepherd, T. G., Shindell, D., Stähelin, J., Tegtmeier, S., Thomason, L., Tilmes, S., Vernier, J.-P., Waugh, D. W. and Young, P. J.: Overview of IGAC/SPARC Chemistry-Climate Model Initiative (CCMI) Community Simulations in Support of Upcoming Ozone and Climate Assessments, SPARC Newsl., 40(January), 48–66, 2013.

Falk, S., Sinnhuber, B.-M., Krysztofiak, G., Jöckel, P., Graf, P., and Lennartz, S. T.: Brominated VSLS and their influence on ozone under a changing climate, Atmos. Chem. Phys., 17, 11313–11329, https://doi.org/10.5194/acp–17–11313–2017, 2017.

Feng, W., Chipperfield, M. P., Dorf, M., Pfeilsticker, K., and Ricaud, P.: Mid-latitude ozone changes: studies with a 3-D CTM forced by ERA-40 analyses, Atmos. Chem. Phys., 7, 2357–2369, https://doi.org/10.5194/acp–7–2357–2007, 2007

Fernandez, R. P., Salawitch, R. J., Kinnison, D. E., Lamarque, J.-F. and Saiz-Lopez, A.: Bromine partitioning in the tropical tropopause layer: implications for stratospheric injection, Atmos. Chem. Phys., 14, 13391–13410, https://doi.org/10.5194/acp–14–13391–2014, 2014.

Fernandez, R. P., Kinnison, D. E., Lamarque, J.–F., Tilmes, S. and Saiz-Lopez, A.: Impact of biogenic very short-lived bromine on the Antarctic ozone hole during the 21st century, Atmos. Chem. Phys., 17, 1673–1688, https://doi.org/10.5194/acp–2016–840, 2017.

Frith, S. M., Kramarova, N. A., Stolarski, R. S., McPeters, R. D., Bhartia, P. K., and Labow, G. J.: Recent changes in total column ozone based on the SBUV Version 8.6 Merged Ozone Data Set, J. Geophys. Res. Atmos., 119, 9735–9751, https://doi.org/10.1002/2014JD021889, 2014.

Frith, S. M., Stolarski, R. S., Kramarova, N. A., and McPeters, R. D.: Estimating uncertainties in the SBUV Version 8.6 merged profile ozone data set, Atmos. Chem. Phys., 17, 14695–14707, https://doi.org/10.5194/acp–17–14695–2017, 2017.

Heckendorn, P., Weisenstein, D., Fueglistaler, S., Luo, B., Rozanov, E., Schraner, M., Thomason, L., and Peter, T.: The impact of geo-engineering aerosols on stratospheric temperature and ozone, Environ. Res. Lett., 4, 045108, https://doi.org/10.1088/1748–9326/4/4/045108, 2009.

Hendrick, F., M. Van Roozendael, M.P. Chipperfield, M. Dorf, F. Goutail, X. Yang, C. Fayt, C. Hermans, K. Pfeilsticker, J.P. Pommereau, J.A. Pyle, N. Theys, and M. De Mazière.: Retrieval of stratospheric and tropospheric BrO profiles and columns using ground-based zenith-sky DOAS observations at Harestua, 60° N, Atmos. Chem. Phys., 7, 4869–4885, https://doi.org/10.5194/acp–7–4869–2007, 2007.

Hendrick, F., Johnston, P. V., Kreher, K., Hermans, C., De Maziere, M., and Van Roozendael, M.: One decade trend analysis of stratospheric BrO over Harestua (60º N) and Lauder (44º S) reveals a decline, Geophys. Res. Lett., 35, L14801, https://doi.org/10.1029/2008GL034154, 2008.

Hossaini, R., Chipperfield, M. P., Saiz-Lopez, A., Harrison, J. J., von Glasow, R., Sommariva, R., Atlas, E.,

Navarro, M., Montzka, S. A., Feng, W., Dhomse, S., Harth, C., Mühle, J., Lunder, C., O'Doherty, S., Young, D., Reimann, S., Vollmer, M. K., Krummel, P. B., and Bernath, P. F.: Growth in stratospheric chlorine from short-lived chemicals not controlled by the Montreal Protocol, Geophys. Res. Lett., 42, 4573–4580, doi:10.1002/2015GL063783, 2015a.

Hossaini, R., M. P. Chipperfield, S. A. Montzka, A. Rap, S. Dhomse, and W. Feng.: Efficiency of short-lived halogens at influencing climate through depletion of stratospheric ozone, Nat. Geosci., 8, 186–190, https://doi.org/ 10.1038/NGEO2363, 2015b.

Hossaini, R., Chipperfield, M. P., Montzka, S. A., Leeson, A. A., Dhomse, S., and Pyle, J. A.: The increasing threat to stratospheric ozone from dichloromethane, Nat. Commun., 8, 15962, https://doi.org/10.1038/ncomms15962, 2017.

Iglesias-Suarez, F., Kinnison, D. E., Rap, A., Maycock, A. C., Wild, O., and Young, P. J.: Key drivers of ozone change and its radiative forcing over the 21st century, Atmos. Chem. Phys., 18, 6121–6139, https://doi.org/10.5194/acp–18–6121–2018, 2018.

Klobas, J. E., Wilmouth, D. M., Weisenstein, D. K., Anderson, J. G., & Salawitch, R. J.: Ozone depletion following future volcanic eruptions, Geophys. Res. Lett., 44, 7490–7499, https://doi.org/10.1002/2017GL073972, 2017.

Lamarque, J.-F., Kinnison, D. E., Hess, P. G., and Vitt, F. M.: Simulated lower stratospheric trends between 1970 and 2005: Identifying the role of climate and composition changes, J. Geophys. Res., 113, D12301, https://doi.org/10.1029/2007JD009277, 2008.

Lamarque, J.-F., Emmons, L. K., Hess, P. G., Kinnison, D. E., Tilmes, S., Vitt, F., Heald, C. L., Holland, E. A., Lauritzen, P. H., Neu, J., Orlando, J. J., Rasch, P. J. and Tyndall, G. K.: CAM-chem: description and evaluation of interactive atmospheric chemistry in the Community Earth System Model, Geosci. Model Dev., 5, 369–411, https://doi.org/10.5194/gmd–5–369–2012, 2012.

Leedham Elvidge, E. C., Oram, D. E., Laube, J. C., Baker, A. K., Montzka, S. A., Humphrey, S., O'Sullivan, D. A., and Brenninkmeijer, C. A. M.: Increasing concentrations of dichloromethane, CH_2Cl_2, inferred from CARIBIC air sam ples collected 1998–2012, Atmos. Chem. Phys., 15, 1939–1958, https://doi.org/10.5194/acp–15–1939–2015, 2015.

Lennartz, S.T., G. Krysztofiak, C.A. Marandino, B.M. Sinnhuber, S. Tegtmeier, F. Ziska, R. Hossaini, K. Krüger, S.A. Montzka, E. Atlas, D.E. Oram, T. Keber, H. Bönisch, and B. Quack.: Modelling marine emissions and atmospheric distributions of halocarbons and dimethyl sulfide: the influence of prescribed water concentration vs. prescribed emissions, Atmos. Chem. Phys., 15, 11753–11772, https://doi.org/10.5194/acp–15–11753–2015, 2015.

Livesey, N. J., Read, W. G., Wagner, P. A., Froidevaux, L., Lambert, A., Manney, G. L., F., L., Valle, M., Pumphrey, H. C., Santee, M. L., Schwartz, M. J., Wang, S., Fuller, R. A., Jarnot, R. F., Knosp, B. W., Martinez, E., and Lay, R. R.: Version 4.2x Level 2 data quality and description document, JPL D–33509, Rev. D., Jet Propulsion Lab, 2018.

Marsh, D. R., Mills, M. J., Kinnison, D. E., Lamarque, J.-F., Calvo, N., and Polvani, L. M.: Climate Change from 1850 to 2005 Simulated in CESM1(WACCM), J. Climate, 26, 7372–7391, https://doi.org/10.1175/JCLI-D-12-00558.1, 2013.

Marsh, D. R., Mills, M. J., Kinnison, D. E., Lamarque, J.-F., Calvo, N., and Polvani, L. M.: Climate Change from 1850 to 2005 Simulated in CESM1(WACCM), J. Climate, 26, 7372–7391, https://doi.org/10.1175/JCLI-D-12-00558.1, 2013.McElroy, M. B., Salawitch, R. J., Wofsy, S. C., and Logan, J. A.: Reductions of Antarctic ozone due to synergistic interactions of chlorine and bromine, Nature, 321, 759–762, 1986.

Meinshausen, M., Smith, S. J., Calvin, K., Daniel, J. S., Kainuma, M. L. T., Lamarque, J. F., Matsumoto, K., Montzka, S. A., Raper, S. C. B., Riahi, K., Thomson, A., Velders, G. J. M., and Vuuren, D. P. P.: The RCP greenhouse gas concentrations and their extensions from 1765 to 2300, Clim. Change, 109, 213–241, https://doi.org/10.1007/s10584–011–0156–z, 2011.

Müller, R. Ed.: Stratospheric Ozone Depletion and Climate Change, RSC Publishing, Cambridge, Chapter 3, 78–99, 2012.

Neale, R. B., Richter, J., Park, S., Lauritzen, P. H., Vavrus, S. J., Rasch, P. J., and Zhang, M.: The Mean Climate of the Community Atmosphere Model (CAM4) in Forced SST and Fully Coupled Experiments, J. Climate, 26, 5150–5168, https://doi.org/10.1175/JCLI-D-12-00236.1, 2013.

Ordóñez, C., Lamarque, J.-F., Tilmes, S., Kinnison, D. E., Atlas, E. L., Blake, D. R., Sousa Santos, G., Brasseur, G. and Saiz-Lopez, A.: Bromine and iodine chemistry in a global chemistry-climate model: description and evaluation of very short-lived oceanic sources, Atmos. Chem. Phys., 12, 1423–1447, https://doi.org/10.5194/acp–12–1423–2012, 2012.

Prather, M. J. and Watson, R. T.: Stratospheric ozone depletion and future levels of atmospheric chlorine and bromine, Nature, 344, 729–734, 1990.

Quack, B. and Wallace, D. W. R.: Air-sea flux of bromoform: Controls, rates, and implications, Global Biochem. Cy., 17, 1023, https://doi.org/10.1029/2002GB001890, 2003.

Quack, B., Peeken, I., Petrick, G., and Nachtigall, K.: Oceanic distribution and sources of bromoform and dibromomethane in the Mauritanian upwelling, J. Geophys. Res., 112, C10006, https://doi.org/10.1029/2006JC003803, 2007.

Riese, M., Ploeger, F., Rap, A., Vogel, B., Konopka, P., Dameris, M., and Forster, P.: Impact of uncertainties in atmospheric mixing on simulated UTLS composition and related radiative effects, J. Geophys. Res. Atmos., 117, D16305, https://doi.org/10.1029/2012jd017751, 2012.

Robrecht, S., Vogel, B., Grooß, J.-U., Rosenlof, K., Thornberry, T., Rollins, A., Krämer, M., Christensen, L., and Müller, R.: Mechanism of ozone loss under enhanced water vapour conditions in the mid-latitude lower stratosphere in summer, Atmos. Chem. Phys., 19, 5805–5833, https://doi.org/10.5194/acp–19–5805–2019, 2019.

Rolf, C., Afchine, A., Bozem, H., Buchholz, B., Ebert, V., Guggenmoser, T., Hoor, P., Konopka, P., Kretschmer,

E., Müller, S., Schlager, H., Spelten, N., Sumińska-Ebersoldt, O., Ungermann, J., Zahn, A., and Krämer, M.: Transport of Antarctic stratospheric strongly dehydrated air into the troposphere observed during the HALO-ESMVal campaign 2012, Atmos. Chem. Phys., 15, 9143–9158, https://doi.org/10.5194/acp–15–9143–2015, 2015.

Saiz-Lopez, A. and von Glasow, R.: Reactive halogen chemistry in the troposphere, Chem. Soc. Rev., 41, 6448–6472, https://doi.org/10.1039/c2cs35208g, 2012.

Saiz-Lopez, A., Fernandez, R. P., Ordóñez, C., Kinnison, D. E., Gómez Martín, J. C., Lamarque, J.-F., and Tilmes, S.: Iodine chemistry in the troposphere and its effect on ozone, Atmos. Chem. Phys., 14, 13119–13143, https://doi.org/10.5194/acp–14–13119–2014, 2014.

Salawitch, R. J., Weisenstein, D. K., Kovalenko, L. J., Sioris, C. E., Wennberg, P. O., Chance, K., Ko, M. K. W., and McLinden, C. A.: Sensitivity of ozone to bromine in the lower stratosphere, Geophys. Res. Lett., 32, L05811, https://doi.org/10.1029/2004GL021504, 2005.

Salawitch, R. J., Canty, T., Kurosu, T., Chance, K., Liang, Q., da Silva, A., Pawson, S., Nielsen, J. E., Rodriguez, J. M., Bhartia, P. K., Liu, X., Huey, L. G., Liao, J., Stickel, R. E., Tanner, D. J., Dibb, J. E., Simpson, W. R., Donohoue, D., Weinheimer, A., Flocke, F., Knapp, D., Montzka, D., Neuman, J. A., Nowak, J. B., Ryerson, T. B., Oltmans, S., Blake, D. R., Atlas, E. L., Kinnison, D. E., Tilmes, S., Pan, L. L., Hendrick, F., Van Roozendael, M., Kreher, K., Johnston, P. V., Gao, R. S., Johnson, B., Bui, T. P., Chen, G., Pierce, R. B., Crawford, J. H., and Jacob, D. J.: A new interpretation of total column BrO during Arctic spring, Geophys. Res. Lett., 37, L21805, https://doi.org/10.1029/2010GL043798, 2010.

Santee, M. L., Manney, G. L., Livesey, N. J., Froidevaux, L., Schwartz, M. J., and Read, W. G.: Trace gas evolution in the lowermost stratosphere from Aura Microwave Limb Sounder measurements, J. Geophys. Res., 116, D18306, https://doi.org/10.1029/2011JD015590, 2011.

Sinnhuber, B.-M., Sheode, N., Sinnhuber, M., Chipperfield, M. P., and Feng, W.: The contribution of anthropogenic bromine emissions to past stratospheric ozone trends: a modelling study, Atmos. Chem. Phys., 9, 2863–2871, https://doi.org/10.5194/acp–9–2863–2009, 2009.

Sinnhuber, B.-M. and Meul, S.: Simulating the impact of emissions of brominated very short lived substances on past stratospheric ozone trends, Geophys. Res. Lett., 2449–2456, https://doi.org/10.1002/2014GL062975, 2015.

Solomon, S., Borrmann, S., Garcia, R. R., Portmann, R., Thomason, L., Poole, L. R., Winker, D., and McCormick, M. P.: Heterogeneous chlorine chemistry in the tropopause region, J. Geophys. Res., 102, 21411–21429, https://doi.org/10.1029/97JD01525, 1997.

Solomon, S.: Stratospheric ozone depletion: A review of concepts and history. Rev. Geosphys., 37, 275–316, https://doi.org/10.1029/1999RG900008, 1999.

Solomon, S., Ivy, D. J., Kinnison, D., Mills, M. J., Neely, R. R., and Schmidt, A.: Emergence of healing in the Antarctic ozone layer, Science, 353, 269–274, https://doi.org/10.1126/science.aae0061, 2016a.

Solomon, S., Kinnison, D., Garcia, R. R., Bandoro, J., Mills, M., Wilka, C., Neely III, R. R., Schmidt, A., Barnes,

J. E., Vernier, J., and Höpfner, M.: Monsoon circulations and tropical heterogeneous chlorine chemistry in the stratosphere, Geophys. Res. Lett., 43, 12624–12633, https://doi.org/10.1002/2016GL071778, 2016b.

Spang, R., Günther, G., Riese, M., Hoffmann, L., Müller, R., and Griessbach, S.: Satellite observations of cirrus clouds in the Northern Hemisphere lowermost stratosphere, Atmos. Chem. Phys., 15, 927–950, https://doi.org/10.5194/acp–15–927–2015, 2015.

Strahan, S. E. and Douglass, A. R.: Decline in Antarctic Ozone Depletion and Lower Stratospheric Chlorine Determined From Aura Microwave Limb Sounder Observations, Geophys. Res. Lett., 45, 382–390, https://doi.org/10.1002/2017GL074830, 2018.

Tilmes, S., Müller, R., & Salawitch, R.: The sensitivity of polar ozone depletion to proposed geoengineering schemes, Science, 320, 1201–1204, https://doi.org/10.1126/science.1153966, 2008.

Tilmes, S., Kinnison, D. E., Garcia, R. R., Salawitch, R., Canty, T., Lee-Taylor, J., Madronich, S., and Chance, K.: Impact of very short-lived halogens on stratospheric ozone abundance and UV radiation in a geo-engineered atmosphere, Atmos. Chem. Phys., 12, 10945–10955, https://doi.org/10.5194/acp–12–10945–2012, 2012.

Tilmes, S., Lamarque, J., Emmons, L. K., Kinnison, D. E., Marsh, D., Garcia, R. R., Smith, A. K., Neely, R. R., Conley, A., Vitt, F., Martin, M. V., Tanimoto, H., Simpson, I., Blake, D. R. and Blake, N.: Representation of the Community Earth System Model (CESM1) CAM4–chem within the Chemistry-Climate Model Initiative (CCMI), Geosci. Model Dev., 9, 1853–1890, https://doi.org/10.5194/gmd–9–1853–2016, 2016.

Thornton, B. F., Toohey, D. W., Avallone, L. M., Harder, H., Martinez, M., Simpas, J. B., Brune, W. H., and Avery, M. A.: In situ observations of ClO near the winter polar tropopause, J. Geophys. Res., 108, 8333, doi:10.1029/2002JD002839, 2003.

von Hobe, M., Grooß, J.-U., Günther, G., Konopka, P., Gensch, I., Krämer, M., Spelten, N., Afchine, A., Schiller, C., Ulanovsky, A., Sitnikov, N., Shur, G., Yushkov, V., Ravegnani, F., Cairo, F., Roiger, A., Voigt, C., Schlager, H., Weigel, R., Frey, W., Borrmann, S., Müller, R., and Stroh, F.: Evidence for heterogeneous chlorine activation in the tropical UTLS, Atmos. Chem. Phys., 11, 241–256, https://doi.org/10.5194/acp–11–241–2011, 2011.

Warwick, N. J., Pyle, J. A., Carver, G. D., Yang, X., Savage, N. H., O'Connor, F. M., and Cox, R. A.: Global modeling of biogenic bromocarbons, J. Geophys. Res., 111, D24305, https://doi.org/10.1029/2006JD007264, 2006

Waters, J. W., Froidevaux, L., Harwood, R. S., Jarnot, R. F., Pickett, H. M., Read, W. G., Siegel, P. H., Cofield, R. E., Filipiak, M. J., Flower, D. A., Holden, J. R., Lau, G. K., Livesey, N. J., Manney, G. L., Pumphrey, H. C., Santee, M. L., Wu, D. L., Cuddy, D. T., Lay, R. R., Loo, M. S., Perun, V. S., Schwartz, M. J., Stek, P. C., Thurstans, R. P., Boyles, M. A., Chandra, K. M., Chavez, M. C., Chen, G. S., Chudasama, B. V., Dodge, R., Fuller, R. A., Girard, M. A., Jiang, J. H., Jiang, Y., Knosp, B. W., Labelle, R. C., Lam, J. C., Lee, K. A., Miller, D., Oswald, J. E., Patel, N. C., Pukala, D. M., Quintero, O., Scaff, D. M., Van Snyder, W., Tope, M. C., Wagner, P. A., and Walch, M. J.: The Earth Observing System Microwave Limb Sounder (EOS MLS) on the Aura

satellite, IEEE T, Geosci. Remote, 44, 1075–1092, https://doi.org/10.1109/TGRS.2006.873771, 2006.

Weber, M., Coldewey-Egbers, M., Fioletov, V. E., Frith, S. M., Wild, J. D., Burrows, J. P., Long, C. S., and Loyola, D.: Total ozone trends from 1979 to 2016 derived from five merged observational datasets – the emergence into ozone recovery, Atmos. Chem. Phys., 18, 2097–2117, https://doi.org/10.5194/acp-18-2097-2018, 2018.

World Meteorological Organization (WMO): Scientific Assessment of Ozone Depletion: 2010. Global Ozone Research and Monitoring Project-Report No. 52, Geneva, Switzerland, 2011.

World Meteorological Organization (WMO): Scientific Assessment of Ozone Depletion: 2014. Global Ozone Research and Monitoring Project-Report No. 55, Geneva, Switzerland, 2014.

World Meteorological Organization (WMO): Scientific Assessment of Ozone Depletion: 2018. Global Ozone Research and Monitoring Project-Report No. 58, Geneva, Switzerland, 2018.

Wofsy, S. C., McElroy, M. B., and Yung, Y. L.: The chemistry of atmospheric bromine, Geophys. Res. Lett., 2, 215–218, https://doi.org/10.1029/GL002i006p00215, 1975.

Yang, X., Abraham, N. L., Archibald, A. T., Braesicke, P., Keeble, J., Telford, P. J., Warwick, N. J., and Pyle, J. A.: How sensitive is the recovery of stratospheric ozone to changes in concentrations of very short-lived bromocarbons?, Atmos. Chem. Phys., 14, 10431–10438, https://doi.org/10.5194/acp–14–10431–2014, 2014.

Ziska, F., B. Quack, S. Tegtmeier, I. Stemmler, and K. Krüger.: Future emissions of marine halogenated very-short lived substances under climate change, J. Atmos. Chem., 74(2), 245–260, https://doi.org/10.1007/s10874–016–9355–3, 2017.

10 Tables and Figures

Table 1: Annual and seasonal TOC changes (ΔTOC) mediated by VSL^{Br} within the mid-latitudes and tropics during the present-day and the end of the 21st century periods, as well as the ΔTOC trends (% dec^{-1}) over century.

Season	Region	ΔTOC^{2000} § DU (%)	ΔTOC^{2100} § DU (%)	ΔTOC trends † (% dec^{-1})
annual mean	NH-ML	– 5.5 ± 0.6 (– 1.6 ± 0.6)	–2.7 ± 0.2 (– 0.8± 0.2)	0.10 ± 0.03
	Trop	– 2.1 ± 0.3 (– 0.8 ± 0.2)	– 1.5 ± 0.1 (– 0.6 ± 0.1)	0.03 ± 0.01
	SH-ML	– 8.0 ± 0.8 (– 2.5 ± 0.3)	– 3.9 ± 0.4 (– 1.2 ± 0.3)	0.15 ± 0.04
DJF	NH-ML	– 6.2 ± 0.1 (– 1.7 ± 0.6)	– 3.2 ± 0.3 (– 0.8 ± 0.2)	0.11 ± 0.03
	Trop	– 2.3 ± 0.3 (– 0.9 ± 0.1)	– 1.8 ± 0.1 (– 0.7 ± 0.1)	0.02 ± 0.01
	SH-ML	– 6.9 ± 0.6 (– 2.4 ± 0.4)	– 4.5 ± 0.2 (– 1.5 ± 0.1)	0.10 ± 0.03
MAM	NH-ML	– 7.7 ± 0.9 (– 2.0 ± 0.6)	– 3.7 ± 0.3 (– 0.9 ± 0.2)	0.14 ± 0.04
	Trop	– 2.1 ± 0.2 (– 0.8 ± 0.2)	– 1.5 ± 0.1 (– 0.6 ± 0.1)	0.02 ± 0.01
	SH-ML	– 6.2 ± 0.5 (– 2.2 ± 0.3)	– 4.2 ± 0.2 (– 1.4 ± 0.1)	0.11 ± 0.03
JJA	NH-ML	– 4.1 ± 0.6 (– 1.3 ± 0.2)	– 2.3 ± 0.2 (– 0.7 ± 0.1)	0.09 ± 0.03
	Trop	– 2.0 ± 0.3 (– 0.8 ± 0.2)	– 1.6 ± 0.1 (– 0.6 ± 0.1)	0.02 ± 0.01
	SH-ML	– 8.0 ± 0.9 (– 2.5 ± 0.2)	– 3.2 ± 0.4 (– 0.9 ± 0.1)	0.19 ± 0.06
SON	NH-ML	– 3.8 ± 0.4 (–1.2 ± 0.1)	– 1.6 ± 0.1 (– 0.5 ± 0.1)	0.10 ± 0.03
	Trop	–1.9 ± 0.2 (–0.7 ± 0.1)	– 1.5 ± 0.1 (– 0.6 ± 0.1)	0.01 ± 0.01
	SH-ML	–10.0 ± 1.2 (–3.0 ± 0.8)	– 5.7 ± 0.4 (– 1.6 ± 0.8)	0.20 ± 0.06

§ Absolute (DU) and relative (%, in brackets) TOC changes during the present-day (ΔTOC^{2000}) and the end of the 21st century (ΔTOC^{2100}) periods were computed considering the mean ensemble of each experiment within the mid-latitudes (SH-ML and NH-ML) and tropics (Trop). Annual and seasonal ΔTOC errors were estimated from standard errors of mean.

† Trend errors were estimated as twice the statistical deviation stemming from the least squares fit.

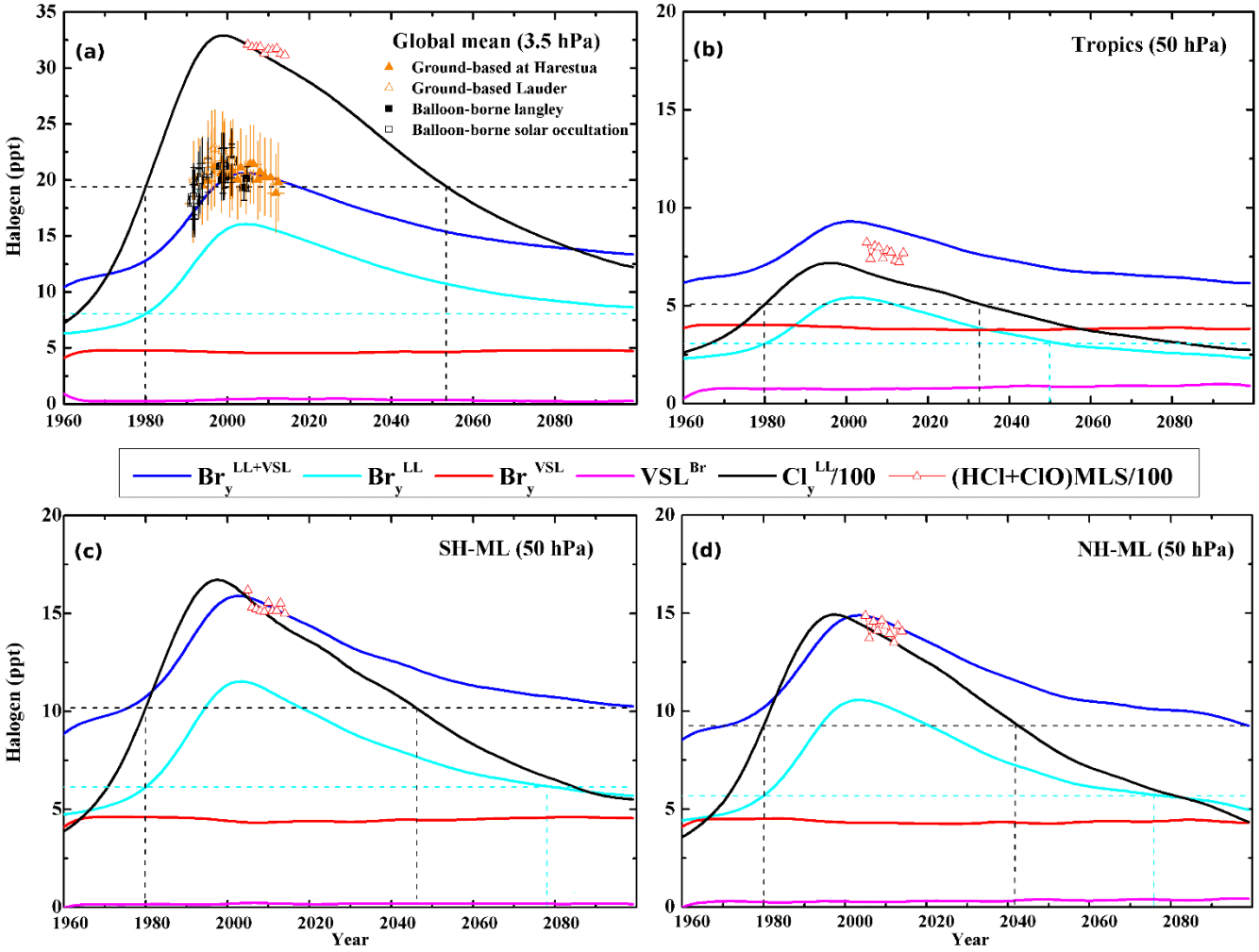

Figure 1: Temporal evolution (1960–2100) of the modelled annual mean abundances of VSL^{Br} and inorganic halogen (Cl_y^{LL} and Br_y^{LL+VSL}): (a) global upper stratosphere (3.5 hPa); lower stratosphere (50 hPa) at (b) Tropics, (c) SH-ML and (d) NH-ML. The Br_y^{LL+VSL} abundance was split into their long-lived (Br_y^{LL}) and very short-lived (Br_y^{VSL}) contributions. The black squares (filled and open) and orange triangles (filled and open) of the panel (a) show the total Br_y evolution (1991-2012) reported in the latest WMO (2014; 2018). The red triangles show the mean annual mixing ratios (HCl + ClO) from the Microwave Limb Sounder (MLS) data (Waters et al., 2006; Livesey et al., 2018) from 2005 to 2015. The dashed horizontal lines indicate the modelled Cl_y^{LL} and Br_y^{LL} abundances for 1980. Note that both Cl_y^{LL} values and (HCl + ClO) MLS data were divided by 100.

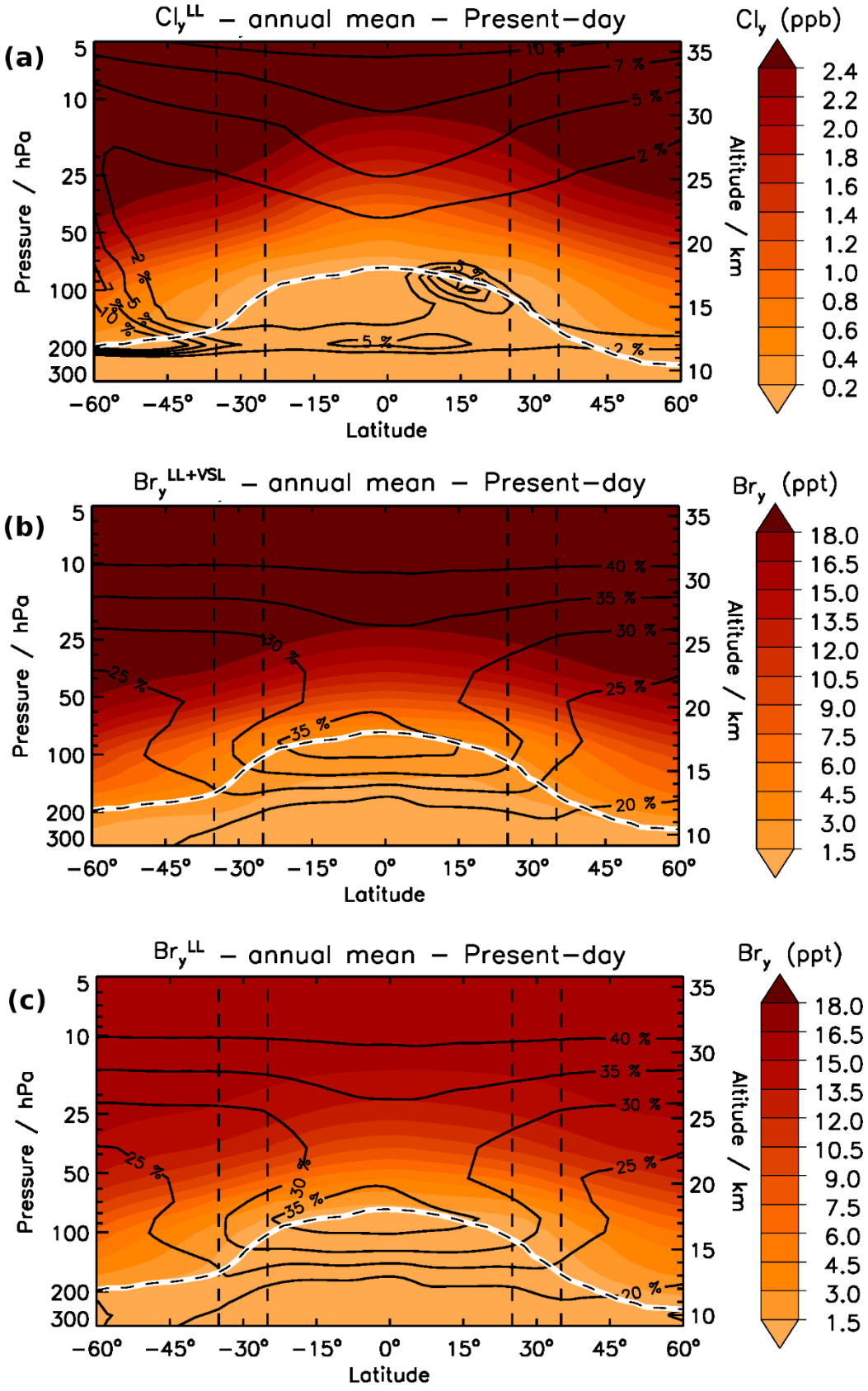

Figure 2: Annual zonal mean distribution of (a) Cl_y^{LL}, (b) Br_y^{LL+VSL} and (c) Br_y^{LL} during the present-day period. The colour scale represents volume mixing ratios (ppb or ppt), while black contour lines show the percentage contribution of ClO_x to Cl_y and BrO_x to Br_y, respectively. The lower solid white line indicates the location of the tropopause (chemical definition of 150 ppb ozone level from experiment without VSL^{Br} sources).

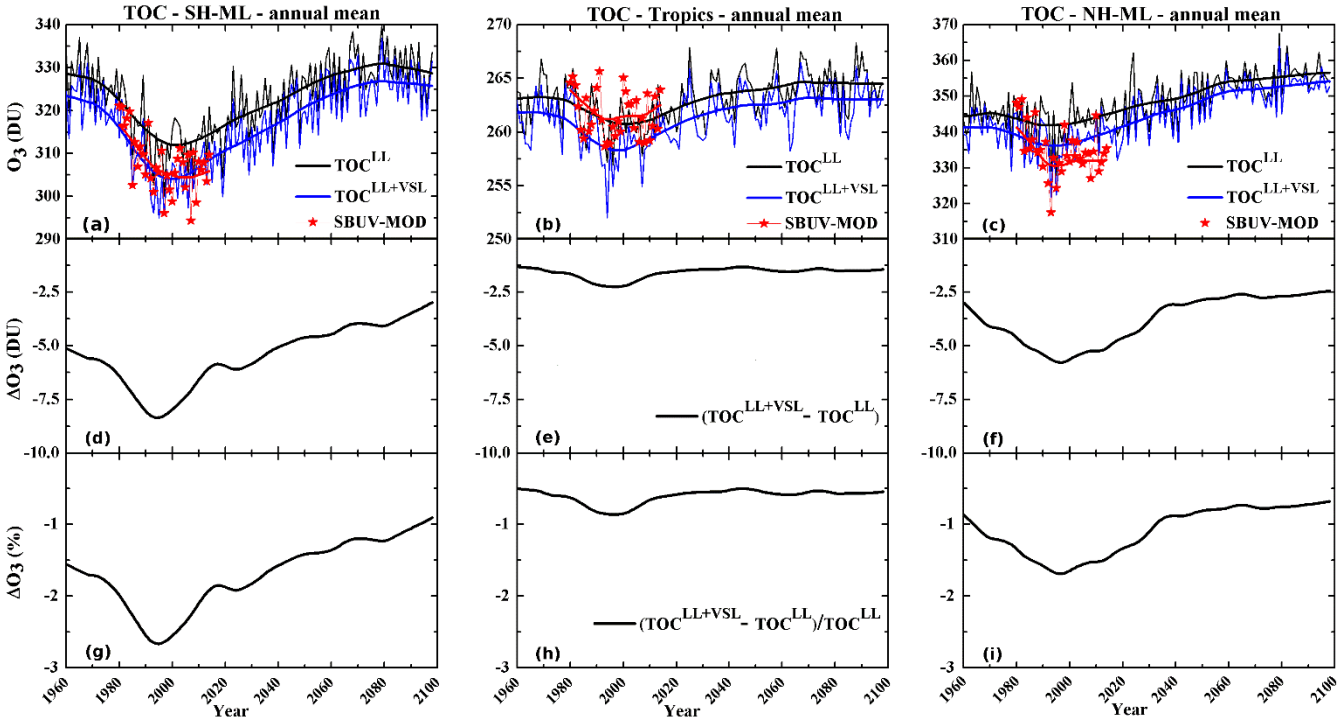

Figure 3: Temporal evolution of the annual mean total ozone column (TOC^{LL+VSL} and TOC^{LL}) within the (a) SH-ML, (b) tropics and (c) NH-ML, as well as the corresponding absolute (DU; d,e,f) and relative (%; g,h,i) TOC difference (ΔTOC). TOC values of the mean ensemble (thin lines) and the time-series smoothed applying a lowess filtering (0.2 fractions; thick lines) are shown in blue for TOC^{LL+VSL} and black for TOC^{LL}. The red lines and symbols show the observations from the Solar Backscatter Ultraviolet (SBUV) merged total ozone column data set (Frith et al., 2014, 2017), within the same spatial and temporal mask as the model output.

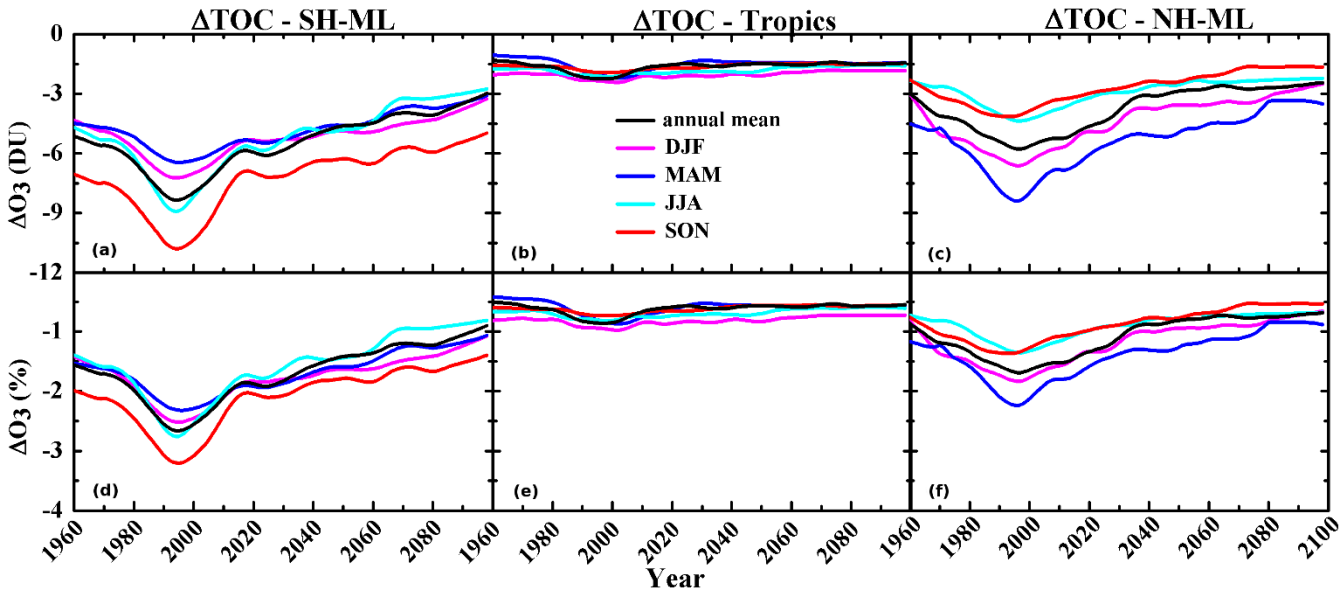

Figure 4: Temporal evolution of total ozone column difference (ΔTOC) between the experiments. The panels (a), (b) and (c) show the annual and seasonal mean absolute ΔTOC (DU) within the SH-ML, tropics and NH-ML, respectively, while the panels (d), (e) and (f) show the corresponding relative ΔTOC (%).

5

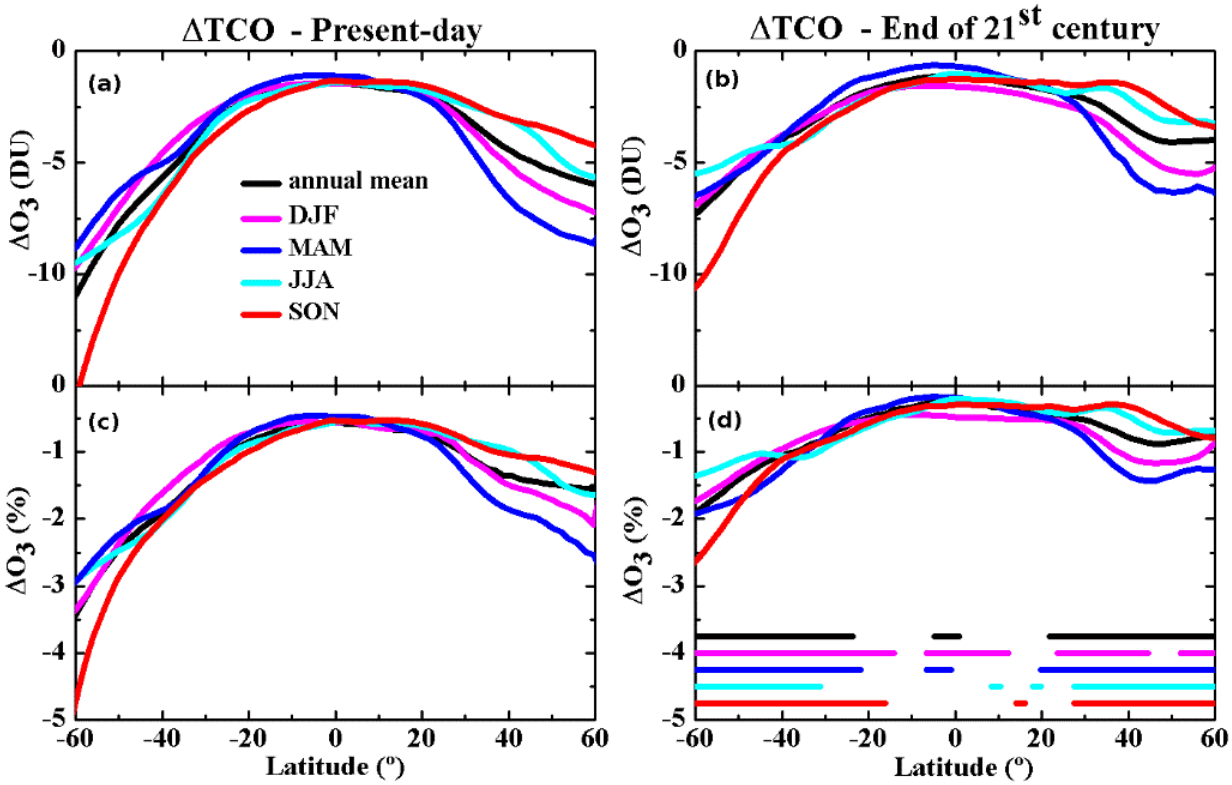

Figure 5: Latitude distributions of total ozone column difference (ΔTOC) between the experiments. The panels (a) and (b) show the annual and seasonal mean absolute ΔTOC (DU) for the present-day and the end of 21st century periods, respectively, while the panels (c) and (d) show the corresponding relative ΔTOC (%). The corresponding horizontal lines shown in panel (d) indicate where the relative ΔTOC between the present-day and the end of the 21st century periods are statistically significant, at the 95% confidence interval using a two-tailed Student's *t* test.

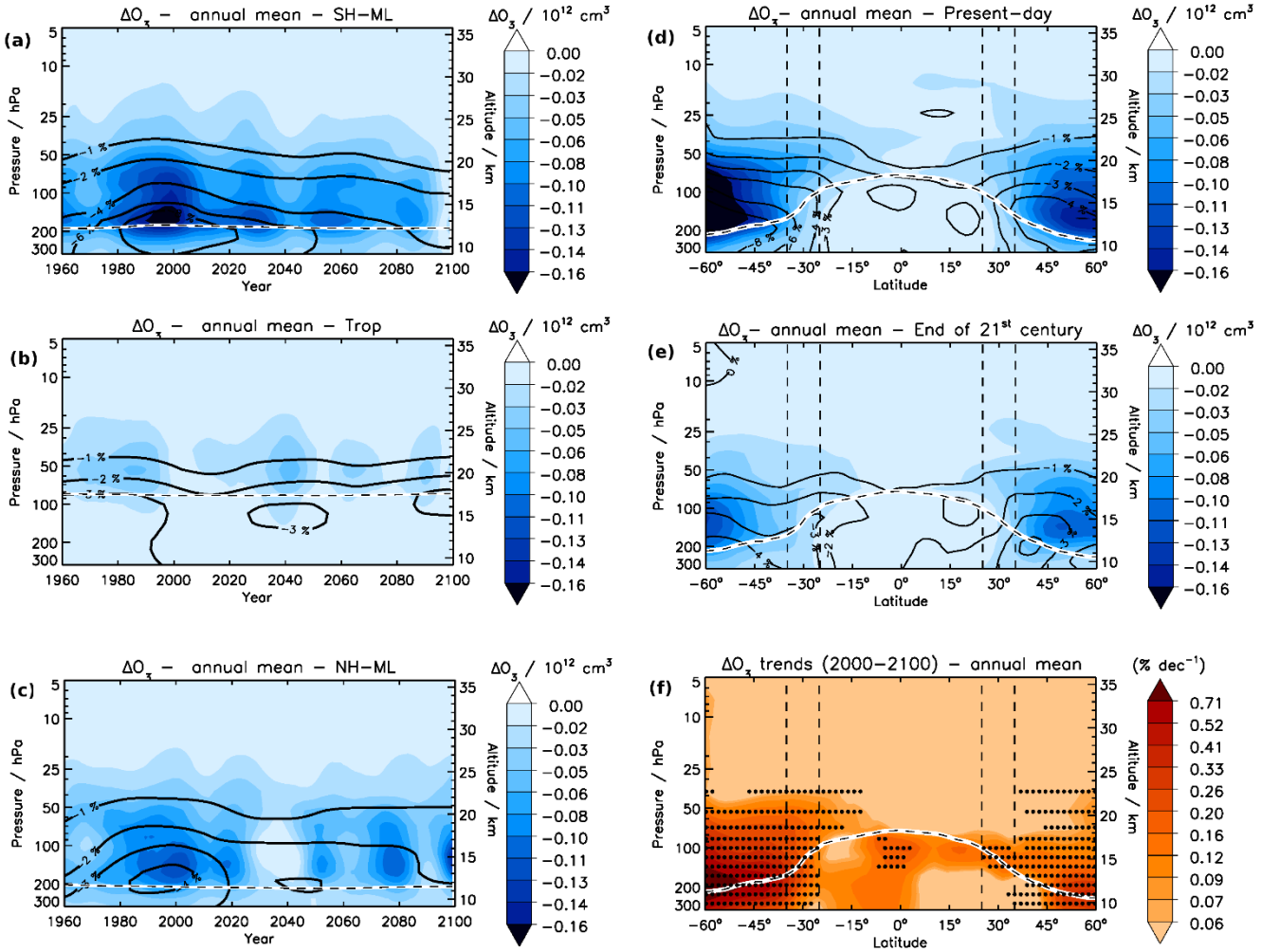

Figure 6: Temporal evolution of the annual mean ozone difference (ΔO_3) between experiments as a function of altitude, within the (a) SH-ML, (b) tropics and (c) NH-ML. The right panels show the zonal mean ΔO_3 distributions for the (d) present-day and (e) the end of the 21st century periods, as well as the (f) ΔO_3 trends (% dec^{-1}) over the century. The absolute (colour scale) and relative (contour line) ozone differences were calculated considering the ozone number densities (i.e. molecule cm^{-3}) of each experiments. The masked regions in panel (f) indicate where the relative $\Delta O_3(z)$ between the present-day and the end of the 21st century periods are statistically significant, at the 95% confidence interval using a two-tailed Student's *t* test.

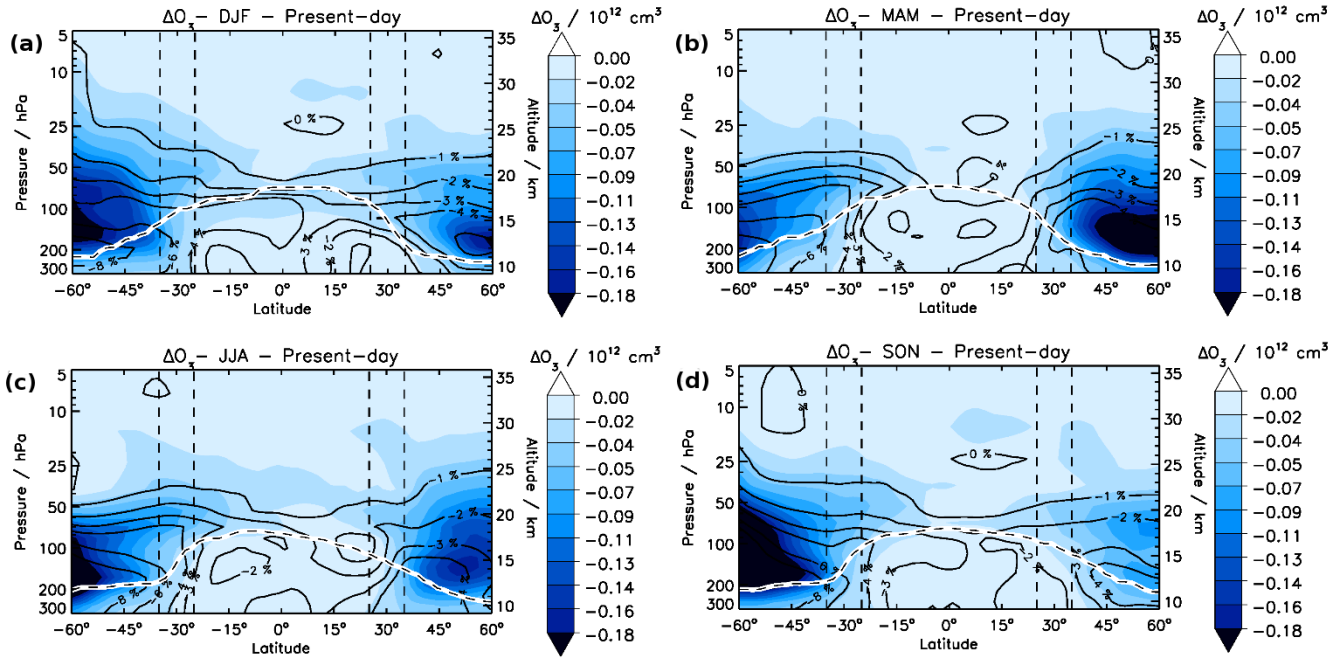

Figure 7: Seasonal zonal mean ΔO_3 distributions during the present-day period.

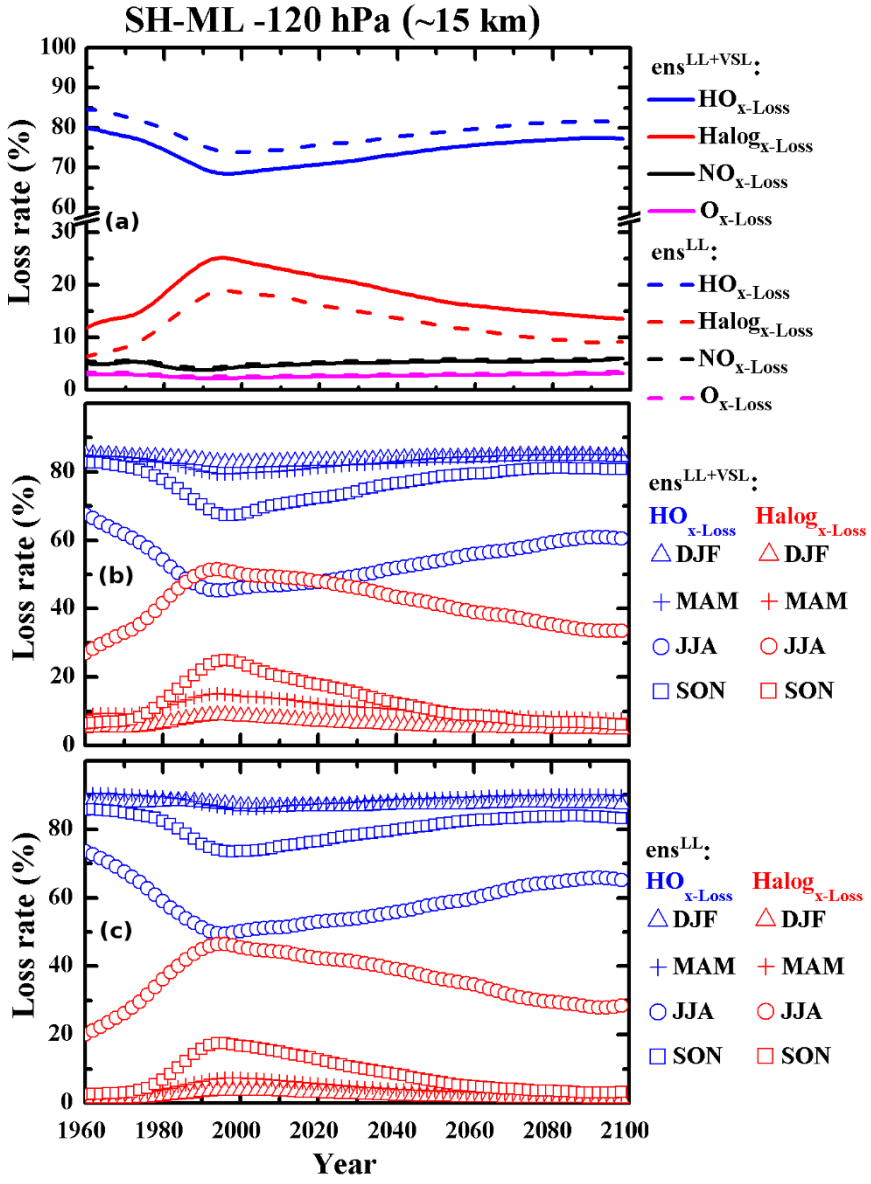

Figure 8: Temporal evolution of the percentage contributions from different ozone-depleting families (O_{x-Loss}, NO_{x-Loss}, HO_{x-Loss}, $Halog_{x-Loss}$) to the total odd-oxygen loss rate, in the SH-ML lowermost stratosphere (120 hPa). Panel (a) shows the annual mean contribution of each ozone-depleting family for the experiments with (solid line; ens^{LL+VSL}) and without (dashed line; ens^{LL}) VSL^{Br} sources. The panels (b) and (c) show the seasonal mean contributions of both HO_{x-Loss} and $Halog_{x-Loss}$ for the experiments with and without VSL^{Br} sources, respectively.

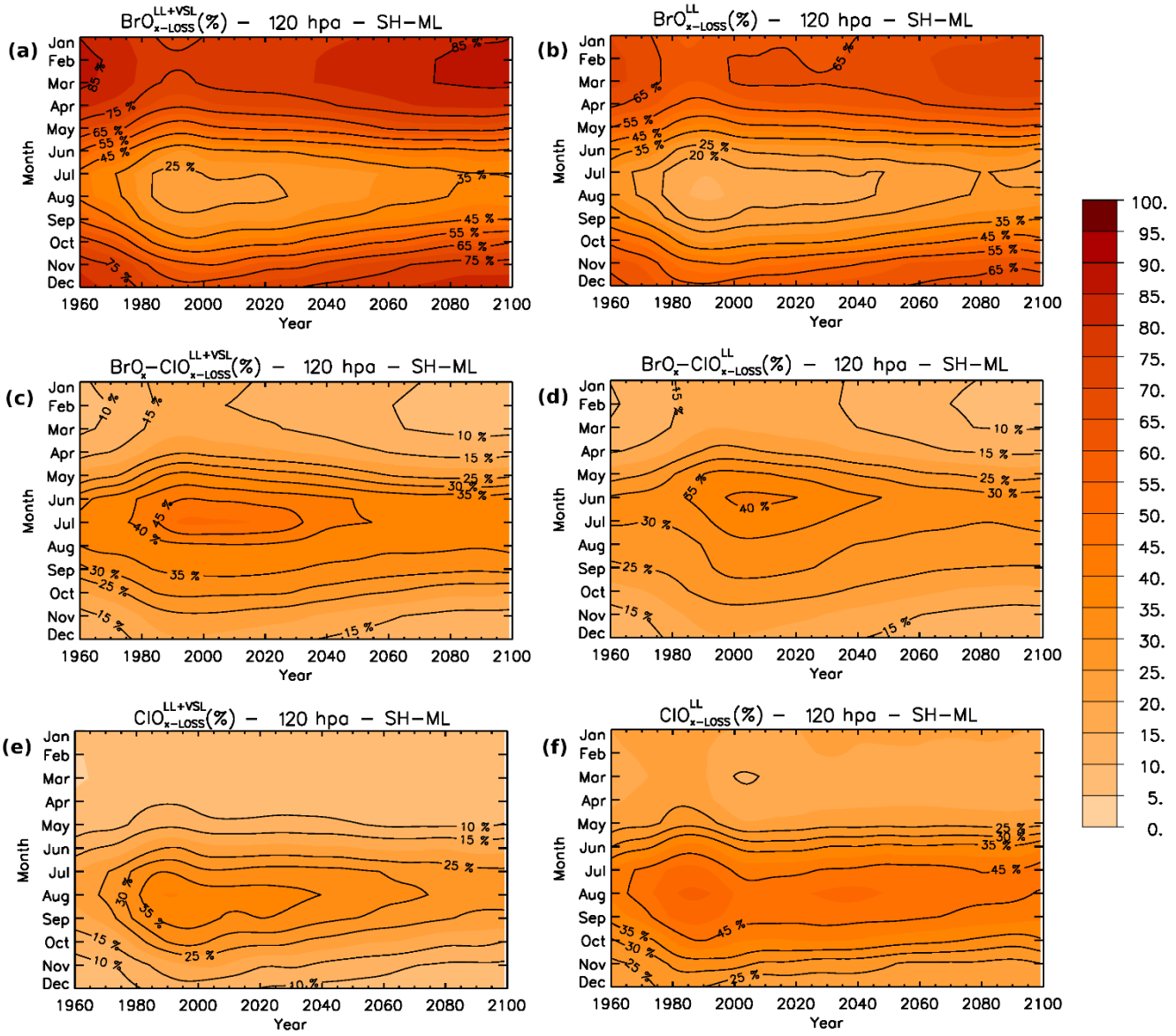

Figure 9: Evolution of the (a,b) BrO_{x-Loss}, (c,d) ClO_x-BrO_{x-Loss} and (e,f) ClO_{x-Loss} percentage contributions to $Halog_{x-Loss}$ as a function of the year and month in the SH-ML lowermost stratosphere (120 hPa), for the experiments with (left panels) and without (right panel) VSL^{Br} sources.

5